

Reconfigurable Intelligent Surface Empowered Device-to-Device Communication Underlying Cellular Networks

Gang Yang, *Member, IEEE*, Yating Liao, *Student Member, IEEE*,
Ying-Chang Liang, *Fellow, IEEE*, Olav Tirkkonen, *Senior Member, IEEE*,
Gongpu Wang, *Member, IEEE*, Xing Zhu, *Member, IEEE*

Abstract—Reconfigurable intelligent surface (RIS) is a new and revolutionary technology to achieve spectrum-, energy- and cost-efficient wireless networks. This paper studies the resource allocation for RIS-empowered device-to-device (D2D) communication underlying a cellular network, in which an RIS is employed to enhance desired signals and suppress interference between paired D2D and cellular links. We maximize the overall network’s spectrum efficiency (SE) and energy efficiency (EE), respectively, by jointly optimizing the spectrum reuse indicators, the transmit power, the RIS’s passive beamforming and the BS’s receive beamforming. To solve both mixed-integer non-linear programming problems, we first propose an efficient and low-complexity user-pairing scheme based on relative channel strength to determine the spectrum reuse indicators. Other variables are then optimized to maximize the SE by an iterative algorithm, based on the techniques of alternating optimization, successive convex approximation, Lagrangian dual transform and quadratic transform. The EE-maximization problem is solved by an

alternating algorithm integrated with Dinkelbach’s method. Numerical results show that the proposed design achieves significant SE and EE enhancements compared to traditional underlay D2D network without RIS, relay-assisted D2D network and other benchmarks.

Index Terms—Device-to-device communication, reconfigurable intelligent surface, spectrum efficiency optimization, energy efficiency optimization, resource allocation, passive beamforming.

I. INTRODUCTION

A. Motivation

Device-to-device (D2D) communication underlying a cellular network allows a device to communicate with proximity devices in licensed cellular bands. It is recognized as a promising wireless technology and a competitive candidate for beyond 5th-Generation (5G) system standards [1]. Specifically, the overall network’s spectrum efficiency (SE) can be enhanced, since additional D2D links are supported by sharing the licensed cellular spectrums; the overall network’s energy efficiency (EE) can be improved by exploiting the proximity of D2D users; also, the transmission delay can be reduced by eliminating the forwarding through a cellular base station (BS). Task offloading in edge computing networks can effectively improve the mobile devices’ computation and energy efficiency [2], [3]. D2D communications is also a promising offloading solution in cellular networks with high SE and EE. However, interference management is an important challenge for underlay D2D communication [1], [4], [5]. The D2D link and the cellular link operating in the same band interfere with each other, and the interference needs to be carefully suppressed via efficient interference control [6] and resource allocation [7]. Existing interference management schemes were designed assuming that the wireless environment including interference channels is fixed. Thus the extent of interference suppression is fundamentally limited.

Recently, reconfigurable intelligent surface (RIS) has emerged as a new and revolutionary technology to achieve

This work was supported by the National Natural Science Foundation of China under Grants 62071093 and U1801261, the National Key R&D Program of China under Grant 2018YFB1801105, the Macau Science and Technology Development Fund (FDCT), Macau SAR, under Grant 0009/2020/A1, the Fundamental Research Funds for the Central Universities under Grant ZYGX2019Z022, and the Programme of Introducing Talents of Discipline to Universities under Grant B20064. The work of Olav Tirkkonen was funded in part by the Academy of Finland (Grant 319484). This work was partly presented in IEEE Wireless Communications and Networking Conference (WCNC), Nanjing, China, 2021.

G. Yang and Y. Liao are with the National Key Laboratory of Science and Technology on Communications, and the Center for Intelligent Networking and Communications (CINC), University of Electronic Science and Technology of China (UESTC), Chengdu 611731, China (e-mails: yanggang@uestc.edu.cn, 2015010913035@std.uestc.edu.cn).

Y.-C. Liang is with the Center for Intelligent Networking and Communications (CINC), University of Electronic Science and Technology of China (UESTC), Chengdu 611731, China (e-mail: liangyc@ieee.org). (*Corresponding author: Y.-C. Liang.*)

O. Tirkkonen is with the Department of Communications and Networking, Aalto University, Aalto FI-00076, Finland (e-mail: olav.tirkkonen@aalto.fi).

G. Wang is with the Beijing Key Laboratory of Transportation Data Analysis and Mining, School of Computer and Information Technology, Beijing Jiaotong University, Beijing 100044, China (e-mail: gp-wang@bjtu.edu.cn).

X. Zhu is with the State Key Laboratory Geohazard Prevention and Geoenvironment Protection, Chengdu University of Technology, Chengdu 610059, China (e-mail: zhuxing15@cdut.edu.cn).

spectrum-, energy- and cost-efficient wireless networks [8]–[10]. An RIS consists of a large number of passive low-cost reflecting elements, each of which can adjust the phase and amplitude of the incident electromagnetic wave in a software-defined way and reflect it passively [11]. Thus, RIS is able to enhance desired signals and suppress interference by designing passive beamforming (i.e., changing each reflecting element’s reflecting coefficient including amplitude and phase). In particular, a typical RIS architecture consists of a smart controller and three layers (i.e., a reflecting element, copper backplane, and a control circuit board) [8]. The controller attached to RIS can intelligently adjust the reflecting coefficients and communicate with other network components. Hence, the wireless propagation environment can be intentionally re-configured, which opens up for fundamental improvements in interference management for underlay D2D communication. Moreover, a full-duplex amplify-and-forward (AF) relay actively processes the received signals and transmits the amplified signals, which leads to additional noise and self-interference at the relay. Therefore, RIS outperforms full-duplex AF relay in terms of EE and cost efficiency [12].

RIS can be explored to not only suppress the severe interference between each paired D2D link and cellular link, but also to enhance the strength of desired signals for both D2D and cellular links. This motivates us to study RIS-empowered D2D communication underlaying a cellular network as shown in Fig. 1, which consists of multiple D2D pairs and multiple cellular users (CUs), as well as an RIS. This RIS-empowered underlay D2D network has not been comprehensively studied in the literature for both SE and EE to our best knowledge. For the related work, the EE of an RIS-assisted pure D2D network without interplay with the cellular network was recently maximized by optimizing only the D2D transmission power and the RIS’s passive beamforming in [13].

B. Related Works

1) *D2D Communication*: The SE maximization with interference management in D2D communication systems were studied in [14]–[16]. For D2D communication underlaying cellular networks, the overall network’s SE was maximized in [14] by jointly optimizing the spectrum reuse indicators and transmit power. For D2D communication underlaying an orthogonal-frequency-division-multiplexing (OFDM) cellular network, the average ergodic sum rate over D2D pairs’ locations was maximized in [15] by jointly optimizing the subcarrier assignment and power allocation. For a direct D2D communication network, a deep learning approach was proposed in [16] to maximize the overall network SE by optimizing the scheduling of D2D links.

Also, the EE maximization or energy minimization with interference management in D2D communication systems

were studied in [17]–[20]. For D2D communication underlaying a multiuser multiple-input multiple-output cellular network, the total transmit power of the overall network was minimized in [17], by jointly optimizing the BS’s transmit beamforming and transmit power of both BS and D2D transmitters. The overall EE of an underlay D2D network, which allows multiple D2D users pair with a CU, was maximized in [18] by jointly optimizing the spectrum reuse indicators and power allocation. The overall EE was maximized in [19] for dedicated transmission mode, reusing transmission mode and cellular transmission mode, while considering the circuit power consumption and the QoS requirements for D2D users and CUs. The performance of an underlay D2D network over fading channels was analyzed in [20] by leveraging a stochastic geometric approach.

The aforementioned works improve SE or EE performance of the underlay D2D communication systems. By optimizing the spectrum reuse indicators, BS’s transmit beamforming or users’ transmit power, these works carefully designed the interference management schemes. However, in these works, the wireless environment is considered to be fixed, and can only be compensated through sophisticated transmission and reception design. In contrast, through the RISs passive beamforming design, our work reconfigures the wireless propagation environment intelligently, thus further enhances the SE and EE performance significantly compared to the aforementioned works.

2) *Wireless Communication with RIS*: Wireless communication systems with RIS can be divided into two categories, i.e., RIS-based transceiver design and RIS-assisted wireless communication. For the former, the RISs are utilized as transmit antennas and receive antennas to significantly reduce the hardware cost of traditional wireless transceivers [21]. Most research belongs to the latter category, in which RIS is applied to improve the performance of wireless systems. RIS has similarities with backscatter communications, with some important differences, however. Backscatter communication enables a tag to deliver its own information to a receiver by intentionally switching the antenna’s load impedances [22] [23], while an RIS is used to enhance the existing communication link performance.

RIS-assisted wireless communication was extensively studied in the prior works. For example, the weighted sum rate of an RIS-aided multiuser multiple-input single-output (MISO) downlink system was maximized in [24], by jointly optimizing the BS’s active beamforming and the RIS’s passive beamforming (i.e., reflecting coefficients). The ergodic sum rate of an RIS-assisted MISO system was maximized in [25] through deep reinforcement learning, by jointly optimizing the BS’s transmit beamforming and the RIS’s phase shifts. For an RIS-assisted downlink

non-orthogonal-multiple-access system, the max-min rate performance was optimized in [26]. The EE of an RIS-empowered downlink multiuser system was maximized in [27], by jointly optimizing the BS's transmit power and the RIS's passive beamforming. Existing works which investigated RIS-assisted multi-user wireless communication did not involve the issue of user pairing. For RIS-empowered underlay D2D communications, since the wireless environment depends on the RIS's passive beamforming design, the user pairing scheme is closely coupled with the RIS's passive beamforming design. The traditional user pairing schemes are thus no longer applicable. This motivates us to propose an efficient user-pairing scheme for RIS-empowered underlay D2D communications.

C. Contributions

In this paper, we study the resource allocation for an RIS-empowered underlay D2D communication network as shown in Fig. 1. Compared with the conference-version paper [28], this work extends the signal-antenna BS to a practical multiple-antenna one, and also investigates the EE-maximization problem. The main contributions are summarized as follows

- We formulate a problem to maximize the overall network SE (i.e., sum rate of D2D users and CUs) [29], by jointly optimizing the spectrum reuse indicators (i.e., user pairing between D2D users and CUs), transmit power, RIS's passive beamforming and BS's receive beamforming. This problem is challenging to solve optimally, since the user pairing involves integer variables and is closely coupled with resource allocation. To our best knowledge, it is the first work to investigate the joint design of user pairing, power allocation and interference suppression via active-and-passive beamforming in the RIS-empowered underlay D2D communication networks.
- To decouple the SE-maximization problem, we first propose an efficient relative-channel-strength (RCS) based user-pairing scheme. Under the obtained user-pairing design, an iterative algorithm based on alternating optimization (AO), successive convex approximations (SCA), Lagrangian dual transform (LDT) and quadratic transform (QT) is further proposed. The algorithm's convergence and complexity are also analyzed. The proposed user-pairing scheme is of low-complexity, and suffers from slight performance degradation compared to the ideal user-pairing benchmark based on high-complexity exhaustive search.
- We propose a practical RIS power-consumption model, which characterizes how the number of reflecting elements and the quantization bits affect the power consumption. Based on this model, we formulate a problem to maximize the overall network EE, by jointly optimizing the spectrum reuse indicators,

transmit power, RIS's passive beamforming and BS's receive beamforming. To solve this non-convex problem, the proposed RCS-based user-pairing scheme is first utilized to determine the spectrum reuse indicators, and an AO-based algorithm integrated with Dinkelbach's method is then proposed to optimize other variables iteratively. We also analyze the algorithms' convergence and complexity.

- Numerical results show that the proposed design achieves significant SE and EE enhancements compared to traditional underlay D2D without RIS, and suffers from slight degradation compared to the best-achievable performance under ideal user pairing. A 3-bit quantized phase shifter achieves sufficient SE enhancement compared to the ideal case of a continuous phase shifters. As the number of reflecting elements increases, the EE monotonically increases in the considered practical parameter setup for the RIS-empowered underlay D2D network, while it increases first and then decreases for relay-assisted underlay D2D network. The effects of other main parameters on performances are also numerically verified.

D. Organization and Notations

The rest of this paper is organized as follows. Section II presents the system model for RIS-empowered underlay D2D communication network. Section III formulates the SE maximization problem, and proposes an RCS-based user-pairing scheme together with an efficient iterative algorithm to solve this problem. Section IV formulates and solves the EE-maximization problem. Section V provides numerical results. Section VI concludes this paper.

The main notations are as follows. We denote scalars, vectors and matrices by italic letters, bold-face lowercase letters and bold-face upper-case letters, respectively, e.g., a , \mathbf{a} , \mathbf{A} . The space of $x \times y$ complex matrices is denoted by $\mathcal{C}^{x \times y}$. The set of real number and positive real numbers are \mathcal{R} and \mathcal{R}^+ , respectively. The distribution of a circularly symmetric complex Gaussian (CSCG) random variable with mean μ and variance σ^2 is $\mathcal{CN}(\mu, \sigma^2)$, and the transpose and conjugate transpose of a vector \mathbf{v} are \mathbf{v}^T and \mathbf{v}^H , respectively. The l_2 -norm notation is denoted by $\|\cdot\|$. We denote the operation of taking real part by $\text{Re}\{\cdot\}$.

II. SYSTEM MODEL

In this section, we first describe the RIS-empowered underlay D2D communication network, and then present the signal model.

A. System Description

As shown in Fig. 1, we consider an RIS-empowered cellular network with underlay D2D, which consists of

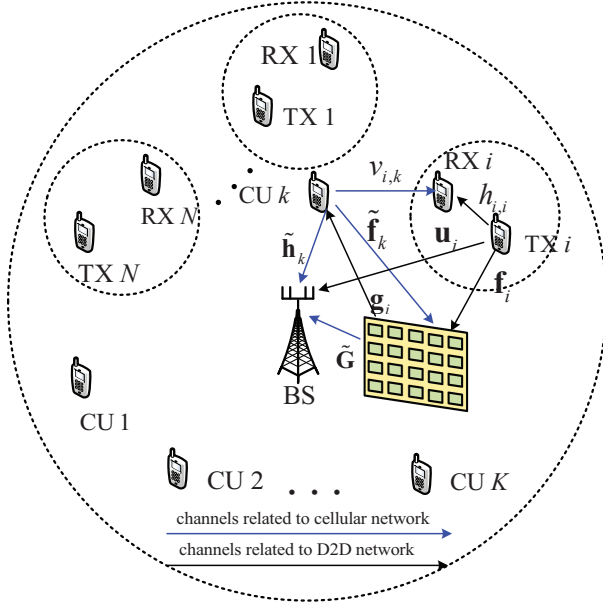


Fig. 1: An RIS-empowered underlay D2D communication network.

an RIS¹, N ($N \geq 1$) D2D transmitters (TXs) denoted as TX 1, ..., TX N , N D2D receivers (RXs) denoted as RX 1, ..., RX N , K active CUs (i.e., cellular users) denoted as CU 1, ..., CU K , and a cellular BS. The BS has Q antennas and the RIS has M ($M \geq 1$) reflecting elements; while each D2D TX, D2D RX and CU are equipped with a single antenna. A controller is attached to the RIS to control the reflecting coefficients and communicate with other network components through separate wireless links. We assume that the D2D links share the uplink (UL) spectrum of the cellular network, since the UL spectrum is typically underutilized compared to the downlink spectrum. To alleviate interference, we assume that a D2D link shares at most one CU's spectrum resource, while the spectrum resource of a CU can be shared by at most one D2D link [14] [31]. To ensure that each D2D link can be paired with one cellular link, we further assume that $K \geq N$.

All channels are assumed to experience quasi-static flat fading. The channels from TX i ($1 \leq i \leq N$) to RX l ($1 \leq l \leq N$) and RIS are denoted by $h_{l,i} \in \mathcal{C}$ and $\mathbf{f}_i \in \mathcal{C}^{M \times 1}$, respectively. For notational clarity, we represent all channels related to the cellular network with a tilde. The channels from CU k ($1 \leq k \leq K$) to BS and RIS are denoted by $\tilde{\mathbf{h}}_k \in \mathcal{C}^{Q \times 1}$ and $\tilde{\mathbf{f}}_k \in \mathcal{C}^{M \times 1}$, respectively; the channels from RIS to RX l and BS are denoted by $\mathbf{g}_l \in \mathcal{C}^{M \times 1}$ and $\tilde{\mathbf{G}} \in \mathcal{C}^{M \times Q}$, respectively; the interference channels from TX i to BS and from CU k to

¹This work can be easily extended to a multiple-RIS setup, through combining multiple phase-shift matrices and RIS-related channel matrices (or vectors) into composite ones, respectively [30], and adopting the same solving methods as in this work.

RX l are denoted by $\mathbf{u}_i \in \mathcal{C}^{Q \times 1}$ and $v_{i,k} \in \mathcal{C}$, respectively. Since RIS is typically a passive device without signal processing capabilities, it is challenging to estimate the individual RIS-related channels. Nevertheless, there are certain efficient algorithms to estimate the RIS-related channels². There are also a few papers investigating the RIS-empowered communication with imperfect CSI³. This paper focuses on system optimization, thus all the channels are assumed to be perfectly known.

B. Signal Model

Let $\Phi = \text{diag}\{\beta_1, \dots, \beta_M\} \in \mathcal{C}^{M \times M}$ denotes the reflecting coefficient matrix of the RIS, where the elements are $\beta_m = \alpha_m e^{j\psi_m}$, in terms of reflecting amplitude $\alpha_m \in \mathcal{R}^+$ and reflecting phase $\psi_m \in \mathcal{R}$, for $1 \leq m \leq M$. The reflecting coefficient β_m belongs to feasible set \mathcal{F} . Denote the reflecting coefficient vector as $\boldsymbol{\theta} = [\beta_1, \dots, \beta_M]^T$. Three different settings for reflecting coefficients are considered in this paper.

1) *Ideal Reflecting Coefficient*: The amplitude and phase of each reflecting element are continuously adjustable, i.e., $\alpha_m \in [0, 1]$ and $\psi_m \in [0, 2\pi)$. The ideal reflecting coefficient set is $\mathcal{F}_1 = \{\beta_m = \alpha_m e^{j\psi_m} \mid |\beta_m| \leq 1\}$.

2) *Continuous Reflecting Phase Shift*: The reflecting phase shift ψ_m takes continuous values in the range $[0, 2\pi)$, and the amplitude is fixed to $\alpha_m = 1$. The continuous reflecting phase shift set is $\mathcal{F}_2 = \{\beta_m = e^{j\psi_m} \mid \psi_m \in [0, 2\pi)\}$.

3) *Discrete Reflecting Phase Shift*: The reflecting phase shift ψ_m is B -bit quantized, taking 2^B discrete values, and the reflecting amplitude⁴ $\alpha_m = 1$. The discrete reflecting phase shift set is $\mathcal{F}_3 = \{\beta_m = e^{j\psi_m} \mid \psi_m \in \{0, \frac{2\pi}{2^B}, \dots, \frac{(2^B-1)2\pi}{2^B}\}\}$.

From [10] [36], by switching different resistor loads and setting different bias voltages to tuning elements like varactor diodes, different reflecting amplitudes and phase shifts can be realized. Due to hardware characteristics and cost limitations, each reflecting element of the RIS typically realizes a finite-resolution phase shift. Nevertheless, it is

²The RIS-related channels can be estimated as discussed in [32] [33]. For instance, an innovative three-phase framework was proposed in [32], which exploited the correlations among the RIS reflected channels to reduce the training overhead. In [33], the BS-to-RIS channel and the RIS-to-user channel are estimated by exploiting sparse matrix factorization and matrix completion, respectively. The RXs are supposed to feed the estimated channels back to the BS.

³With imperfect CSI, the transmit power is minimized in [34] for an RIS-aided MISO communication system, under the bounded CSI error model the statistical CSI error model. In [35], an online stochastic algorithm is developed, which satisfies QoS constraints stochastically without requiring prior knowledge of CSI errors.

⁴Notice that the amplitude is typically smaller than 1 due to the power consumption at the resistance of phase-shift tuning element, and depends on the phase shift in practice [36]. For simplicity and convenience of system optimization, we assume $\alpha_m = 1$.

still valuable to evaluate the system performance with \mathcal{F}_1 and \mathcal{F}_2 , which provides upper-bound performances for \mathcal{F}_3 .

The transmit signals from TX i and CU k , $s_i \sim \mathcal{CN}(0, 1)$ and $x_k \sim \mathcal{CN}(0, 1)$, follow independent CSCG distribution with zero mean and unit variance. Denote the index set of active D2D pairs as $\mathcal{D} \subseteq \{1, \dots, N\}$. The corresponding SINR for RX n decoding s_n from D2D TX $n \in \mathcal{D}$ is

$$\gamma_n^d = \frac{P_n^d |\mathbf{g}_n^H \Phi \mathbf{f}_n + h_{n,n}|^2}{\sum_{k=1}^K \rho_{k,n} P_k^c |\mathbf{g}_n^H \Phi \tilde{\mathbf{f}}_k + v_{n,k}|^2 + \sigma^2}, \quad (1)$$

where P_i^d and P_k^c are the transmit power of TX i and CU k ; $\rho_{k,n}$ is the spectrum reuse indicator for cellular link k and D2D link n , $\rho_{k,n} = 1$ when D2D link n reuses the resource of CU k , and $\rho_{k,n} = 0$ otherwise; σ^2 is the power of additive white Gaussian noise (AWGN) at RX n . For convenience, we denote the length- $(K+N)$ power allocation vector as $\mathbf{p} = [P_1^d, \dots, P_N^d, P_1^c, \dots, P_K^c]^T$, and the length- (KN) spectrum reuse indicator vector as $\boldsymbol{\rho} = [\rho_{1,1}, \dots, \rho_{1,N}, \rho_{2,1}, \dots, \rho_{K,N}]^T \in \mathcal{C}^{Q \times K}$.

The SINR for the BS decoding x_k from CU k is

$$\gamma_k^c = \frac{P_k^c |\mathbf{w}_k (\tilde{\mathbf{G}}^H \Phi \tilde{\mathbf{f}}_k + \tilde{\mathbf{h}}_k)|^2}{\sum_{i=1}^N \rho_{k,i} P_i^d |\mathbf{w}_k (\tilde{\mathbf{G}}^H \Phi \mathbf{f}_i + \mathbf{u}_i)|^2 + \sigma^2 \|\mathbf{w}_k\|^2}, \quad (2)$$

where $\mathbf{w}_k \in \mathcal{C}^{1 \times Q}$ denotes the receive beamforming vector, and σ^2 is the power of AWGN at the BS. The receive beamforming matrix is denoted as $\mathbf{W} = [\mathbf{w}_1^T, \dots, \mathbf{w}_K^T]$.

As defined as the amount of transmitted information by utilizing unit bandwidth in [29], the overall network's SE (i.e., sum rate of both D2D users and CUs) in bps/Hz is

$$R(\boldsymbol{\rho}, \mathbf{p}, \Phi, \mathbf{W}) = \sum_{n \in \mathcal{D}} \log_2(1 + \gamma_n^d) + \sum_{k=1}^K \log_2(1 + \gamma_k^c). \quad (3)$$

III. SPECTRUM EFFICIENCY MAXIMIZATION

In this section, we formulate a problem to maximize the SE in (3), by jointly optimizing the spectrum reuse indicator vector $\boldsymbol{\rho}$, the transmit power vector \mathbf{p} , the reflecting coefficients matrix Φ , and the receive beamforming matrix \mathbf{W} . The optimization problem is formulated as follows

$$(P1): \quad \max_{\boldsymbol{\rho}, \mathbf{p}, \Phi, \mathbf{W}} \quad R(\boldsymbol{\rho}, \mathbf{p}, \Phi, \mathbf{W}) \quad (4a)$$

$$\text{s.t.} \quad \gamma_n^d \geq \gamma_{\min}^d, \quad n \in \mathcal{D} \quad (4b)$$

$$\gamma_k^c \geq \gamma_{\min}^c, \quad 1 \leq k \leq K \quad (4c)$$

$$\rho_{k,n} \in \{0, 1\} \quad (4d)$$

$$\sum_{k=1}^K \rho_{k,n} \leq 1 \quad (4e)$$

$$\sum_{n \in \mathcal{D}} \rho_{k,n} \leq 1 \quad (4f)$$

$$0 \leq P_n^d \leq P_{\max}^d \quad (4g)$$

$$0 \leq P_k^c \leq P_{\max}^c \quad (4h)$$

$$\|\mathbf{w}_k\|^2 \leq 1 \quad (4i)$$

$$\beta_m \in \mathcal{F}, \quad 1 \leq m \leq M \quad (4j)$$

where (4b) and (4c) indicate QoS constraints in terms of required minimum SINRs γ_{\min}^d and γ_{\min}^c for D2D links and cellular links, respectively; (4e) ensures that a D2D link shares at most one CU's resource, while (4f) indicates that the resource of a CU can be shared by at most one D2D link; (4g) and (4h) are the maximum transmit power constraints on the TXs and CUs, respectively; (4i) is the constraint on BS's receive beamforming; and (4j) is the constraint on the reflecting coefficients with $\mathcal{F} \in \{\mathcal{F}_1, \mathcal{F}_2, \mathcal{F}_3\}$.

Note that (P1) is a mixed-integer non-linear program (MINLP), and thus NP-hard. Moreover, the objective function and the constraint functions of (4b) and (4c) are non-concave with respect to the variables $\boldsymbol{\rho}$, \mathbf{p} , Φ and \mathbf{W} , and these variables are all coupled. There is no standard method to solve such a MINLP. In the sequel, we first propose a user-pairing scheme with low complexity to determine the spectrum reuse indicator vector $\boldsymbol{\rho}$. Then, to solve the remaining non-convex problem with the continuous variables, we propose an efficient algorithm based on the alternating optimization (AO), successive convex approximation (SCA), Lagrangian dual transform (LDT) and quadratic transform (QT) techniques to optimize \mathbf{p} , Φ and \mathbf{W} in an iterative manner. To begin with, we solve (P1) with $\mathcal{F} = \mathcal{F}_1$, which makes (4j) a convex constraint. Afterwards, we utilize the projection method to obtain heuristic solutions to (P1) with $\mathcal{F} = \mathcal{F}_2$ and $\mathcal{F} = \mathcal{F}_3$.

A. Relative-Channel-Strength based Pairing Scheme

Since the user-pairing design involves integer programming which is hard to solve, we propose a RCS (i.e., relative-channel-strength) based low-complexity pairing scheme to design the spectrum reuse indicators $\boldsymbol{\rho}$.

From the user-pairing assumptions described in Subsection II-A, there are A_K^N different possible pairings that form the set $\Pi \triangleq \{\pi_1, \dots, \pi_{A_K^N}\}$, with the number of permutations $A_K^N = K(K-1) \cdots (K-N+1)$. Each possible pairing can be viewed as an index mapping $\pi_q: k \in \mathcal{U}_q \rightarrow n \in \mathcal{D}_q$, for $q = 1, \dots, A_K^N$, i.e., the π_q maps each CU index $k \in \mathcal{U}_q \subset \{1, 2, \dots, K\}$ to a D2D-link index $n \in \mathcal{D}_q \subset \mathcal{D}$. The RCS-based pairing scheme determines the pairing π_{q^*} by the following criterion

$$\pi_{q^*} = \arg \max_{\pi_q \in \Pi} \sum_{k \in \mathcal{U}_q} \frac{\|\tilde{\mathbf{h}}_k\|^2}{|v_{\pi_q(k), k}|^2} + \frac{|h_{\pi_q(k), \pi_q(k)}|^2}{\|\mathbf{u}_{\pi_q(k)}\|^2}. \quad (5)$$

This heuristic pairing scheme chooses the pairing mapping which maximizes the sum of the relative channels that is defined as the ratio of (transmitter-to-receiver) useful channel strength over interference channel strength. Specifically, the first term in the summation of (5) is the ratio of each paired CU-to-BS channel strength over the paired CU-to-RX interference channel strength, and the second term is the ratio of each paired TX-to-RX channel strength over the paired TX-to-BS interference channel strength. The basic guideline for the proposed RCS-based pairing scheme is to pair the users with both large useful-channel strength and small interference-channel strength. To implement this pairing scheme, the BS needs to estimate its channel with each D2D TX, and each D2D RX needs to estimate its channel with each CU and then feed it back to the BS.

This heuristic pairing scheme that requires only simple comparisons has low computational complexity. The resultant design only suffers from slight performance degradation compared to the design with ideal pairing achieved by exhaustive search, as numerically shown in Section V. This RCS-based pairing scheme will also be used for EE maximization in Section IV.

B. Optimize Transmit Power Vector \mathbf{p}

Once the discrete pairing is found, the remaining variables will be optimized iteratively and alternately. In each iteration j , for given reflecting coefficient matrix $\Phi^{(j)}$ and receive beamforming matrix $\mathbf{W}^{(j)}$, the transmit power vector \mathbf{p} can be optimized by solving the following subproblem

$$(P1.1) : \max_{\mathbf{p}} R(\mathbf{p}) \quad (6a)$$

$$\text{s.t. } (4b), (4c), (4g), (4h). \quad (6b)$$

Since the objective function of (P1.1) is not concave with respect to the optimization variable \mathbf{p} , (P1.1) is non-convex. The objective function can be rewritten as follows

$$R = \sum_{n \in \mathcal{D}} \left[\log_2 \left(P_n^d Q_{n,n}^{(j)} + A_1 \right) - \log_2 (A_1) \right] + \sum_{k=1}^K \left[\log_2 \left(P_k^c Q_k^{(j)} + A_2 \right) - \log_2 (A_2) \right], \quad (7)$$

where $Q_{n,n} = |\mathbf{g}_n^H \Phi \mathbf{f}_n + h_{n,n}|^2$, $\tilde{Q}_{n,k} = |\mathbf{g}_n^H \Phi \tilde{\mathbf{f}}_k + v_{n,k}|^2$, $\tilde{Q}_k = |\mathbf{w}_k^H (\tilde{\mathbf{G}}^H \Phi \tilde{\mathbf{f}}_k + \mathbf{h}_k)|^2$, $Q_i = |\mathbf{w}_k^H (\tilde{\mathbf{G}}^H \Phi \mathbf{f}_i + \mathbf{u}_i)|^2$, $A_1 = \sum_{k=1}^K \rho_{k,n} P_k^c \tilde{Q}_{n,k}^{(j)} + \sigma^2$ and $A_2 = \sum_{i=1}^N \rho_{k,i} P_i^d Q_i^{(j)} + \sigma^2 \|\mathbf{w}_k^{(j)}\|^2$.

The non-convexity of (7) comes from the terms $-\log_2(A_1)$ and $-\log_2(A_2)$. We exploit the SCA technique [37] to solve (P1.1). Specifically, from the fact that any convex function can be lower bounded by its first-order Taylor expansion at any point, we obtain the following

concave lower bound R^{lb} at the local point $\mathbf{p}^{(j)}$

$$R \geq \sum_{n \in \mathcal{D}} \left[\log_2 \left(P_n^d Q_{n,n}^{(j)} + A_1 \right) - \log_2 \left(A_1^{(j)} \right) - \frac{1}{A_1^{(j)}} \sum_{k=1}^K \rho_{k,n} \tilde{Q}_{n,k}^{(j)} \left(P_k^c - P_k^{c(j)} \right) \right] + \sum_{k=1}^K \left[\log_2 \left(P_k^c \tilde{Q}_k^{(j)} + A_2 \right) - \log_2 \left(A_2^{(j)} \right) - \frac{1}{A_2^{(j)}} \sum_{i=1}^N \rho_{k,i} Q_i^{(j)} \left(P_i^d - P_i^{d(j)} \right) \right] \triangleq R^{\text{lb}}. \quad (8a)$$

With given local point $\mathbf{p}^{(j)}$ and lower bound R^{lb} , the subproblem (P1.1) is approximated as

$$(P1.1.A) : \max_{\mathbf{p}} R^{\text{lb}} \quad (9a)$$

$$\text{s.t. } (4b), (4c), (4g), (4h). \quad (9b)$$

Problem (P1.1.A) is a convex problem which can be efficiently solved with standard toolbox, e.g., CVX [38]. Notice that the adopted lower bound R^{lb} implies that the feasible set of (P1.1.A) is always a subset of that of (P1.1). As a result, the optimal objective value obtained from (P1.1.A) is in general a lower bound to that of (P1.1).

C. Optimize Reflecting Coefficient Matrix Φ with $\mathcal{F} = \mathcal{F}_1$

In each iteration j , for given transmit power vector $\mathbf{p}^{(j)}$ and receive beamforming matrix $\mathbf{W}^{(j)}$, the reflecting coefficient matrix Φ can be optimized by solving the following subproblem

$$(P1.2) : \max_{\Phi} R(\Phi) \quad (10a)$$

$$\text{s.t. } (4b), (4c), (4j). \quad (10b)$$

In this subsection, we utilize the LDT (i.e., Lagrangian dual transform) [39] and QT (i.e., quadratic transform) [39] techniques to convert (P1.2) into a quadratic constrained quadratic programming (QCQP) problem, and the introduced auxiliary variables are obtained from $\Phi^{(j)}$ in closed forms.

As the first step, the LDT technique is exploited to convert the sum-logarithm objective function $R(\Phi)$ to a sum-fraction expressions. Specifically, introducing auxiliary variables $\boldsymbol{\eta}^d = [\eta_1^d, \dots, \eta_N^d]^T$ and $\boldsymbol{\eta}^c = [\eta_1^c, \dots, \eta_K^c]^T$, the subproblem (P1.2) can be equivalently reformulated as

$$(P1.2.L) : \max_{\Phi, \boldsymbol{\eta}^d, \boldsymbol{\eta}^c} R_a(\Phi, \boldsymbol{\eta}^d, \boldsymbol{\eta}^c) \quad (11a)$$

$$\text{s.t. } (4b), (4c), (4j), \quad (11b)$$

where the new objective function $R_a(\Phi, \boldsymbol{\eta}^d, \boldsymbol{\eta}^c)$ is expressed as

$$R_a = \left(\sum_{n \in \mathcal{D}} \log(1 + \eta_n^d) - \sum_{n \in \mathcal{D}} \eta_n^d + \sum_{n \in \mathcal{D}} \frac{(1 + \eta_n^d) \gamma_n^d}{1 + \gamma_n^d} \right)$$

$$+ \left(\sum_{k=1}^K \log(1 + \eta_k^c) - \sum_{k=1}^K \eta_k^c + \sum_{k=1}^K \frac{(1 + \eta_k^c) \gamma_k^c}{1 + \gamma_k^c} \right). \quad (12a)$$

We proceed by first optimizing η_n^d and η_k^c with fixed γ_n^d and γ_k^c ; then we optimize η_n^d and γ_k^c with fixed η_n^d and η_k^c . It can be easily checked that R_a is a concave differentiable function over η_n^d with fixed γ_n^d , so the optimal value of η_n^d can be obtained by setting $\partial R_a(\gamma_n^{d(j)})/\partial \eta_n^d = 0$, i.e., $\eta_{\text{opt},n}^d = \gamma_n^{d(j)}$. Similarly, $\eta_{\text{opt},k}^c = \gamma_k^{c(j)}$. Replacing η_n^d and η_k^c with $\eta_{\text{opt},n}^d$ and $\eta_{\text{opt},k}^c$, respectively, we find that the optimal objective values of (P1.2) and (P1.2.L) are equal, i.e., $R_a = R$.

We define $\theta^H \omega_{n,n} = \mathbf{g}_n^H \Phi \mathbf{f}_n$, $\theta^H \tilde{\omega}_{n,k} = \mathbf{g}_n^H \Phi \tilde{\mathbf{f}}_k$, $\theta^H \tilde{\omega}_k = \mathbf{w}_k^{(j)H} \tilde{\mathbf{G}}^H \Phi \tilde{\mathbf{f}}_k$ and $\theta^H \omega_i = \mathbf{w}_k^{(j)H} \tilde{\mathbf{G}}^H \Phi \mathbf{f}_i$. From (1) and (2), optimizing the reflecting coefficient matrix Φ can be equivalently transformed into optimizing θ in the following objective function

$$R_b(\theta) = \sum_{n \in \mathcal{D}} \frac{(1 + \eta_{\text{opt},n}^{d(j)}) P_n^{d(j)} Q_{n,n}^w}{P_n^{d(j)} Q_{n,n}^w + \sum_{k=1}^K \rho_{k,n} P_k^{c(j)} \tilde{Q}_{n,k}^w + \sigma^2} + \sum_{k=1}^K \frac{(1 + \eta_{\text{opt},k}^{c(j)}) P_k^{c(j)} \tilde{Q}_k^w}{P_k^{c(j)} \tilde{Q}_k^w + \sum_{i=1}^N \rho_{k,i} P_i^{d(j)} Q_i^w + \sigma^2 \|\mathbf{w}_k^{(j)}\|^2}, \quad (13)$$

where $Q_{n,n}^w = |\theta^H \omega_{n,n} + h_{n,n}|^2$, $\tilde{Q}_{n,k}^w = |\theta^H \tilde{\omega}_{n,k} + v_{n,k}|^2$, $\tilde{Q}_k^w = |\theta^H \tilde{\omega}_k + \mathbf{w}_k^{(j)H} \tilde{\mathbf{h}}_k|^2$ and $Q_i^w = |\theta^H \omega_i + \mathbf{w}_k^{(j)H} \mathbf{u}_i|^2$. Hence, (P1.2.L) can be equivalently reformulated as follows

$$(P1.2.T) : \max_{\theta} R_b(\theta) \quad (14a)$$

$$\text{s.t. (4b), (4c), (4j).} \quad (14b)$$

As the second step, we utilize the QT technique [39] to further convert the multiple-ratio fractional programming problem (P1.2.T) into a QCQP problem. Specifically, introducing the auxiliary variable $\mathbf{y} = [y_1^d, \dots, y_N^d, y_1^c, \dots, y_K^c]^T$, the objective function of (P1.2.T) can be transformed as follows

$$R_c(\theta, \mathbf{y}) = \sum_{n \in \mathcal{D}} \left[2 \sqrt{(1 + \eta_{\text{opt},n}^{d(j)}) P_n^{d(j)}} \text{Re} \left\{ (y_n^d)^* \sqrt{Q_{n,n}^w} \right\} - |y_n^d|^2 \left(P_n^{d(j)} Q_{n,n}^w + \sum_{k=1}^K \rho_{k,n} P_k^{c(j)} \tilde{Q}_{n,k}^w + \sigma^2 \right) \right] + \sum_{k=1}^K \left[2 \sqrt{(1 + \eta_{\text{opt},k}^{c(j)}) P_k^{c(j)}} \text{Re} \left\{ (y_k^c)^* \sqrt{\tilde{Q}_k^w} \right\} - |y_k^c|^2 \left(P_k^{c(j)} \tilde{Q}_k^w + \sum_{i=1}^N \rho_{k,i} P_i^{d(j)} Q_i^w + \sigma^2 \|\mathbf{w}_k^{(j)}\|^2 \right) \right]. \quad (15)$$

We can first optimize \mathbf{y} with fixed θ , then optimize

θ with fixed \mathbf{y} . It can be easily checked that $R_c(\theta, \mathbf{y})$ is a concave differentiable function over \mathbf{y} with fixed θ , so the optimal solution of \mathbf{y} can be obtained by setting $\partial R_c(\mathbf{y}, \theta^{(j)})/\partial \mathbf{y} = 0$. Thus, the optimal values of \mathbf{y} are given by

$$y_{\text{opt},n}^{d(j)} = \frac{\sqrt{(1 + \eta_{\text{opt},n}^{d(j)}) P_n^{d(j)} Q_{n,n}^w}}{P_n^{d(j)} Q_{n,n}^w + \sum_{k=1}^K \rho_{k,n} P_k^{c(j)} \tilde{Q}_{n,k}^w + \sigma^2}, \quad (16)$$

$$y_{\text{opt},k}^{c(j)} = \frac{\sqrt{(1 + \eta_{\text{opt},k}^{c(j)}) P_k^{c(j)} \tilde{Q}_k^w}}{P_k^{c(j)} \tilde{Q}_k^w + \sum_{i=1}^N \rho_{k,i} P_i^{d(j)} Q_i^w + \sigma^2 \|\mathbf{w}_k^{(j)}\|^2}. \quad (17)$$

Substituting the above optimal $y_{\text{opt},n}^{d(j)}$ and $y_{\text{opt},k}^{c(j)}$ into (15), the resulting objective function $R_c(\theta)$ can be formally written as the following quadratic expression

$$R_c(\theta) = -\theta^H \mathbf{B}_1 \theta + 2 \text{Re}(\theta^H \mathbf{e}_1) + C_1, \quad (18)$$

where C_1 is a constant, the matrix \mathbf{B}_1 and vector \mathbf{e}_1 are given by

$$\mathbf{B}_1 = \sum_{n \in \mathcal{D}} \left| y_{\text{opt},n}^{d(j)} \right|^2 (\mathbf{B}_{1n} + \mathbf{B}_{2n}) + \sum_{k=1}^K \left| y_{\text{opt},k}^{c(j)} \right|^2 (\mathbf{B}_{1b} + \mathbf{B}_{2b}), \quad (19a)$$

$$\mathbf{e}_1 = \sum_{n \in \mathcal{D}} \left[\sqrt{(1 + \eta_{\text{opt},n}^{d(j)}) P_n^{d(j)}} (y_{\text{opt},n}^{d(j)})^* \omega_{n,n} - \left| y_{\text{opt},n}^{d(j)} \right|^2 (\mathbf{e}_{1n} + \mathbf{e}_{2n}) \right] + \sum_{k=1}^K \left[\sqrt{(1 + \eta_{\text{opt},k}^{c(j)}) P_k^{c(j)}} (y_{\text{opt},k}^{c(j)})^* \tilde{\omega}_k - \left| y_{\text{opt},k}^{c(j)} \right|^2 (\mathbf{e}_{1b} + \mathbf{e}_{2b}) \right], \quad (19b)$$

with the matrices $\mathbf{B}_{1n} = P_n^{d(j)} \omega_{n,n} \omega_{n,n}^H$, $\mathbf{B}_{2n} = \sum_{k=1}^K \rho_{k,n} P_k^{c(j)} \tilde{\omega}_{n,k} \tilde{\omega}_{n,k}^H$, $\mathbf{B}_{1b} = P_k^{c(j)} \tilde{\omega}_k \tilde{\omega}_k^H$, $\mathbf{B}_{2b} = \sum_{i=1}^N \rho_{k,i} P_i^{d(j)} \omega_i \omega_i^H$, and the vectors $\mathbf{e}_{1n} = P_n^{d(j)} h_{n,n}^* \omega_{n,n}$, $\mathbf{e}_{2n} = \sum_{k=1}^K \rho_{k,n} P_k^{c(j)} v_{n,k}^* \tilde{\omega}_{n,k}$, $\mathbf{e}_{1b} = P_k^{c(j)} (\mathbf{w}_k^{(j)H} \tilde{\mathbf{h}}_k)^* \tilde{\omega}_k$ and $\mathbf{e}_{2b} = \sum_{i=1}^N \rho_{k,i} P_i^{d(j)} (\mathbf{w}_k^{(j)H} \mathbf{u}_i)^* \omega_i$.

Similar to the objective function $R_b(\theta)$ in (P1.2.T), the constraint functions of (4b) and (4c) can be transformed through the QT technique. Specifically, introducing auxiliary variables x_d and x_c , the left hand sides of (4b) and (4c) can be equivalently written as

$$f_d(\theta, x_d) = 2 \sqrt{P_n^{d(j)}} \text{Re} \left((x_d)^* \sqrt{Q_{n,n}^w} \right) - |x_d|^2 \left(\sum_{k=1}^K \rho_{k,n} P_k^{c(j)} \tilde{Q}_{n,k}^w + \sigma^2 \right), \quad (20a)$$

$$f_c(\theta, x_c) = 2 \sqrt{P_k^{c(j)}} \text{Re} \left((x_c)^* \sqrt{\tilde{Q}_k^w} \right)$$

$$-|x_c| \left(\sum_{i=1}^N \rho_{k,i} P_i^{d(j)} Q_i^w + \sigma^2 \|\mathbf{w}_k^{(j)}\|^2 \right). \quad (20b)$$

With fixed $\boldsymbol{\theta}$, $f_d(x_d, \boldsymbol{\theta}^{(j)})$ and $f_c(x_c, \boldsymbol{\theta}^{(j)})$ are concave differentiable functions over x_d and x_c , respectively. The optimal solution of x_d and x_c can be obtained by setting $\partial f_d(x_d, \boldsymbol{\theta}^{(j)})/\partial x_d = 0$ and $\partial f_c(x_c, \boldsymbol{\theta}^{(j)})/\partial x_c = 0$, respectively, and they are given as follows

$$x_{\text{opt},d}^{(j)} = \frac{\sqrt{P_n^{d(j)} Q_{n,n}^{w(j)}}}{\sum_{k=1}^K \rho_{k,n} P_k^{c(j)} \tilde{Q}_{n,k}^w + \sigma^2} \quad (21)$$

$$x_{\text{opt},c}^{(j)} = \frac{\sqrt{P_k^{c(j)} \tilde{Q}_k^{w(j)}}}{\sum_{i=1}^N \rho_{k,i} P_i^{d(j)} Q_{b,i}^w + \sigma^2 \|\mathbf{w}_k^{(j)}\|^2}. \quad (22)$$

By substituting $x_{\text{opt},d}^{(j)}$ and $x_{\text{opt},c}^{(j)}$ in (20a) and (20b), the constraints (4b) and (4c) are equivalent to the following constraints

$$f_d(\boldsymbol{\theta}) = -\boldsymbol{\theta}^H \mathbf{B}_2 \boldsymbol{\theta} + 2\text{Re}(\boldsymbol{\theta}^H \mathbf{e}_2) + C_2 \geq \gamma_{\min}^d, \quad (23a)$$

$$f_c(\boldsymbol{\theta}) = -\boldsymbol{\theta}^H \mathbf{B}_3 \boldsymbol{\theta} + 2\text{Re}(\boldsymbol{\theta}^H \mathbf{e}_3) + C_3 \geq \gamma_{\min}^c, \quad (23b)$$

where the positive-definite matrixes $\mathbf{B}_2 = |x_{\text{opt},d}^{(j)}|^2 \mathbf{B}_{2n}$, $\mathbf{B}_3 = |x_{\text{opt},c}^{(j)}|^2 \mathbf{B}_{2b}$; the vectors $\mathbf{e}_2 = \sqrt{P_n^{d(j)}} \times (x_{\text{opt},d}^{(j)})^* \boldsymbol{\omega}_{n,n} - |x_{\text{opt},d}^{(j)}|^2 \mathbf{e}_{2n}$, $\mathbf{e}_3 = \sqrt{P_k^{c(j)}} (x_{\text{opt},c}^{(j)})^* \tilde{\mathbf{w}}_k - |x_{\text{opt},c}^{(j)}|^2 \mathbf{e}_{2b}$; and the constants $C_2 = 2\sqrt{P_n^{d(j)}} \times \text{Re}\left\{(x_{\text{opt},d}^{(j)})^* h_{n,n}\right\} - |x_{\text{opt},d}^{(j)}|^2 \left(\sum_{k=1}^K \rho_{k,n} P_k^{c(j)} |v_{n,k}|^2 + \sigma^2\right)$ and $C_3 = 2\sqrt{P_k^{c(j)}} \text{Re}\left\{(x_{\text{opt},c}^{(j)})^* \mathbf{w}_k^{(j)} \tilde{\mathbf{h}}_k\right\} - |x_{\text{opt},c}^{(j)}|^2 \left(\sum_{i=1}^N \rho_{k,i} P_i^{d(j)} |\mathbf{w}_k^{(j)} \mathbf{u}_i|^2 + \sigma^2 \|\mathbf{w}_k^{(j)}\|^2\right)$.

Therefore, from (18), (P1.2.T) is transformed as the following QCQP problem

$$(P1.2.Q) : \max_{\boldsymbol{\theta}} -\boldsymbol{\theta}^H \mathbf{B}_1 \boldsymbol{\theta} + 2\text{Re}(\boldsymbol{\theta}^H \mathbf{e}_1) \quad (24a)$$

$$\text{s.t.} \quad (23a), (23b), (4j). \quad (24b)$$

Problem (P1.2.Q) can be effectively solved by standard toolbox like CVX [38].

D. Optimize Receive Beamforming Matrix with $\mathcal{F} = \mathcal{F}_1$

In each iteration j , for given transmit power vector $\mathbf{p}^{(j)}$ and reflecting coefficient matrix $\Phi^{(j)}$, the receive beamforming matrix \mathbf{W} can be optimized by solving the following subproblem

$$(P1.3) : \max_{\mathbf{W}} R(\mathbf{W}) \quad (25a)$$

$$\text{s.t.} \quad (4c), (4i). \quad (25b)$$

The techniques of LDT and QT are utilized to solve (P1.3) once again. The details are omitted herein. By

Algorithm 1 Proposed algorithm for solving (P1)

Step 1: Initialize $\mathbf{p}^{(0)}$, $\Phi^{(0)}$, $\mathbf{W}^{(0)}$, a small threshold constant $\epsilon = 10^{-3}$. Let $j = 0$.

Step 2: Exploit RCS-based pairing scheme to determine the spectrum reuse indicator vector $\boldsymbol{\rho}^*$.

repeat

Step 3: Solve (P1.1.A) for given $\Phi^{(j)}$ and $\mathbf{W}^{(j)}$, and obtain the optimal solution as $\mathbf{p}^{(j+1)}$.

Step 4: Solve (P1.2.Q) for given $\mathbf{p}^{(j+1)}$ and $\mathbf{W}^{(j)}$, and obtain the optimal solution as $\Phi^{(j+1)}$.

Step 5: Solve (P1.3.Q) for given $\mathbf{p}^{(j+1)}$ and $\Phi^{(j+1)}$, and obtain the optimal solution as $\mathbf{W}^{(j+1)}$.

Step 6: Update iteration index $j = j + 1$.

until The increase of objective value is smaller than ϵ .

Step 7: Return the suboptimal solution $\boldsymbol{\rho}^*$, $\mathbf{p}^* = \mathbf{p}^{(j-1)}$, $\Phi^* = \Phi^{(j-1)}$ and $\mathbf{W}^* = \mathbf{W}^{(j-1)}$.

defining $\mathbf{q}_k = \tilde{\mathbf{G}}^H \Phi^{(j)} \tilde{\mathbf{f}}_k + \mathbf{h}_k$ and $\mathbf{q}_{k,i} = \tilde{\mathbf{G}}^H \Phi^{(j)} \mathbf{f}_i + \mathbf{u}_i$, (P1.3) can be equivalently written as follows

$$(P1.3.Q) : \max_{\mathbf{W}} \sum_{k=1}^K [\mathbf{w}_k^H \mathbf{B}_4 \mathbf{w}_k + 2\text{Re}\{\mathbf{w}_k^H \mathbf{e}_{4b}\}] \quad (26a)$$

$$\text{s.t.} \mathbf{w}_k^H (-|\zeta_k^*|^2 \mathbf{B}_{4n}) \mathbf{w}_k + 2\text{Re}\{\mathbf{w}_k^H \mathbf{e}_{4n}\} \geq \gamma_{\min}^d \quad (26b)$$

$$(4i), \quad (26c)$$

where $\zeta_k = \frac{\sqrt{(1+\gamma_k^{(j)}) P_k^{c(j)} \mathbf{w}_k^{(j)} \mathbf{q}_k}}{P_k^{c(j)} |\mathbf{w}_k^{(j)} \mathbf{q}_k|^2 + \sum_{i=1}^N \rho_{k,i} P_i^{d(j)} |\mathbf{w}_k^{(j)} \mathbf{q}_{k,i}|^2 + \sigma^2 \|\mathbf{w}_k^{(j)}\|^2}$,

$\xi_k = \frac{\sqrt{P_k^{c(j)} \mathbf{w}_k^{(j)} \mathbf{q}_k}}{\sum_{i=1}^N \rho_{k,i} P_i^{d(j)} |\mathbf{w}_k^{(j)} \mathbf{q}_{k,i}|^2 + \sigma^2 \|\mathbf{w}_k^{(j)}\|^2}$, $\mathbf{B}_{4n} = \left(\sum_{i=1}^N \rho_{k,i} P_i^{d(j)} \mathbf{q}_{k,i} \mathbf{q}_{k,i}^H\right) + \sigma^2 \mathbf{I}$, $\mathbf{B}_{4b} = P_k^{c(j)} \mathbf{q}_k \mathbf{q}_k^H$,

$\mathbf{B}_4 = -|\zeta_k^*|^2 (\mathbf{B}_{4n} + \mathbf{B}_{4b})$, $\mathbf{e}_{4n} = \sqrt{P_k^{c(j)}} \xi_k^* \mathbf{q}_k$, and $\mathbf{e}_{4b} = \sqrt{(1+\gamma_k^{(j)}) P_k^{c(j)}} \zeta_k^* \mathbf{q}_k$.

(P1.3.Q) is also a QCQP problem, which can be effectively solved by standard toolbox.

E. Overall Algorithm with Convergence and Complexity Analyses

The overall algorithm is summarized in Algorithm 1. There are four blocks of variables to be optimized, i.e., $\boldsymbol{\rho}$, \mathbf{p} , Φ and \mathbf{W} . We first use a low-complexity user-pairing scheme based on the RCS to determine the spectrum reuse indicator vector $\boldsymbol{\rho}$. Under the obtained user-pairing design, we use the AO (i.e., alternating optimization) technique to optimize \mathbf{p} , Φ and \mathbf{W} alternatively in an outer iteration.

Problem (P1) with $\mathcal{F} = \mathcal{F}_2$ and $\mathcal{F} = \mathcal{F}_3$ makes (4j) a non-convex constraint. We utilize the projection method to solve this non-convex problem. For the convenience, the optimal solutions to reflecting coefficient matrix with $\mathcal{F} = \mathcal{F}_1$, $\mathcal{F} = \mathcal{F}_2$ and $\mathcal{F} = \mathcal{F}_3$ are denoted by Φ_1^* , Φ_2^* and Φ_3^* , respectively. We project Φ_1^* into Φ_2^* and Φ_3^* , and

the corresponding elements are given by

$$\Phi_{m,2}^* = e^{j\angle\Phi_{m,1}^*}, \quad (27)$$

$$\Phi_{m,3}^* = \arg \min_{\psi_m \in \{0, \frac{2\pi}{2^B}, \dots, \frac{(2^B-1)2\pi}{2^B}\}} |\psi_m - \angle\Phi_{m,1}^*|, \quad (28)$$

where $\Phi_{m,1}^*$, $\Phi_{m,2}^*$ and $\Phi_{m,3}^*$ denote the m -th diagonal element of Φ_1^* , Φ_2^* and Φ_3^* , respectively.

Theorem 1. *Algorithm 1 is guaranteed to converge.*

Proof: First, in Step 3, since the suboptimal solution $\mathbf{p}^{(j+1)}$ is obtained for given $\Phi^{(j)}$ and $\mathbf{W}^{(j)}$, we have the following inequality on the sum rate

$$\begin{aligned} R(\mathbf{p}^{(j)}, \Phi^{(j)}, \mathbf{W}^{(j)}) &\stackrel{(a)}{=} R^{\text{lb}}(\mathbf{p}^{(j)}, \Phi^{(j)}, \mathbf{W}^{(j)}) \\ &\stackrel{(b)}{\leq} R^{\text{lb}}(\mathbf{p}^{(j+1)}, \Phi^{(j)}, \mathbf{W}^{(j)}) \\ &\stackrel{(c)}{=} R(\mathbf{p}^{(j+1)}, \Phi^{(j)}, \mathbf{W}^{(j)}), \end{aligned} \quad (29)$$

where (a) and (c) hold since the Taylor expansion in (8a) is tight at given local point $\mathbf{p}^{(j)}$ and $\mathbf{p}^{(j+1)}$, and (b) comes from the fact that $\mathbf{p}^{(j+1)}$ is the optimal solution to problem (P1.1.A).

Second, in Step 4 and Step 5, since $\Phi^{(j+1)}$ and $\mathbf{W}^{(j+1)}$ are the optimal solution to (P1.2.Q) and (P1.3.Q), respectively, we can obtain the following inequalities

$$R(\mathbf{p}^{(j+1)}, \Phi^{(j)}, \mathbf{W}^{(j)}) \leq R(\mathbf{p}^{(j+1)}, \Phi^{(j+1)}, \mathbf{W}^{(j)}), \quad (30)$$

$$R(\mathbf{p}^{(j+1)}, \Phi^{(j+1)}, \mathbf{W}^{(j)}) \leq R(\mathbf{p}^{(j+1)}, \Phi^{(j+1)}, \mathbf{W}^{(j+1)}). \quad (31)$$

From (29), (30) and (31), it is straightforward that

$$R(\mathbf{p}^{(j)}, \Phi^{(j)}, \mathbf{W}^{(j)}) \leq R(\mathbf{p}^{(j+1)}, \Phi^{(j+1)}, \mathbf{W}^{(j+1)}), \quad (32)$$

which implies that the objective value of (P1) is non-decreasing after each iteration in Algorithm 1. In addition, the objective value of (P1) is upper-bounded by some finite positive number since the objective function is continuous over the compact feasible set. Hence, the objective values form a Cauchy sequence, and Algorithm 1 is guaranteed to converge. ■

In Algorithm 1, the subproblems (P1.1.A), (P1.2.Q) and (P1.3.Q) are alternatively solved in each outer-layer AO iteration, and the overall complexity of Algorithm 1 is mainly introduced by the update of \mathbf{p} , Φ , \mathbf{W} and auxiliary variables. Since all optimal values of the introduced auxiliary variables are in closed forms, the computational complexity is negligible. Specifically, (P1.1.A) can be solved in $\mathcal{O}((N+K)^3)$ operations [40], while (P1.2.Q) and (P1.3.Q) are convex QCQP which can be solved using interior point methods with complexity $\mathcal{O}(M^{3.5})$ and $\mathcal{O}(Q^{3.5})$, respectively [41]. Hence, the complexity of Algorithm 1 is $\mathcal{O}(I_{\text{ite}}[(N+K)^3 + M^{3.5} + Q^{3.5}])$, where

I_{ite} denotes the number of outer-layer AO iterations. As numerically shown later in Section V, I_{ite} takes the typical value of 5 in general.

IV. ENERGY EFFICIENCY MAXIMIZATION

In this section, we maximize the EE of the overall network, by jointly optimizing the spectrum reuse indicator vector $\boldsymbol{\rho}$, the transmit power vector \mathbf{p} , the reflecting coefficients matrix Φ , and the receive beamforming matrix \mathbf{W} .

A. Problem Formulation for EE Maximization

Before formulating the EE-maximization problem, we model the power consumption of the RIS. Due to the passive reflecting characteristic, the RIS's power consumption mainly comes from the control circuits [27]. For typical control circuits, a field programmable gate array (FPGA) outputs digital control voltages with given sampling frequency, which are converted into analog control voltages by multiple digital-to-analog converters (DACs). The analog control voltage from each DAC adjusts the capacitance of each varactor diode in a continuous way, and thus controls the phase shift and amplitude of each element's reflected signals [27]. Hence, the power consumption of RIS is modeled as follows

$$P_{\text{RIS}}(B) = P_{\text{FPGA}} + MP_{\text{DAC}}(B) + MP_V(B), \quad (33)$$

where P_{FPGA} , $P_{\text{DAC}}(B)$ and $P_V(B)$ denote the power of the FPGA, a B -bit DAC, and a varactor diode with 2^B different bias voltages, respectively. From [42], the DAC's power $P_{\text{DAC}}(B) = 1.5 \times 10^{-5} \cdot 2^B + 9 \times 10^{-12} \cdot B \cdot f_s$, where f_s is the sampling frequency. The varactor-diode power⁵ $P_V(B) = \mathbb{E}_{v_b \in \mathcal{V}}[v_b i_r]$, where $\mathcal{V} = \{V_1, V_2, \dots, V_{2^B}\}$ is the set of designed bias voltages.

Hence, the EE-maximization optimization problem is formulated as

$$(P2): \max_{\boldsymbol{\rho}, \mathbf{p}, \Phi, \mathbf{W}} \frac{R(\boldsymbol{\rho}, \mathbf{p}, \Phi, \mathbf{W})}{\sum_{k=1}^K P_k^c + \sum_{n \in \mathcal{D}} P_n^d + (K+2N+1)P_0 + P_{\text{RIS}}(B)} \quad (34a)$$

$$\text{s.t. (4b), (4c), (4d), (4e), (4f), (4g), (4h), (4i), (4j), \quad (34b)$$

where $\sum_{k=1}^K P_k^c$ and $\sum_{n \in \mathcal{D}} P_n^d$ are the total transmit power of CUs and D2D transmitters, respectively, and P_0 is the circuit-power consumption at each transmitter or receiver of the overall network.

The constraints of (P2) are the same as in (P1). They are non-convex, and the objective function of (P2) is a

⁵Notice that $P_V(B)$ is negligible in practice, since the current of a varactor diode in the reversely-biased (until reverse breakdown) working status is almost constant and very small (typically, tens of nanoAmperes (nA)).

fractional non-convex function. Hence, there is no standard method to solve (P2).

B. Solution to (P2)

To solve (P2), we first determine ρ through the RCS-based user-pairing scheme. Then, the variables \mathbf{p} , Φ and \mathbf{W} are decoupled through AO technique.

1) *Solution to Subproblems:* In each iteration j , for given reflecting coefficient matrix $\Phi^{(j)}$ and receive beamforming matrix $\mathbf{W}^{(j)}$, the transmit power vector \mathbf{p} can be optimized by solving the following problem

$$(P2.1) : \max_{\mathbf{p}} \frac{R(\mathbf{p})}{\sum_{k=1}^K P_k^c + \sum_{n \in \mathcal{D}} P_n^d + (K+2N+1)P_0 + P_{\text{RIS}}(B)}$$

$$\text{s.t. (4b), (4c), (4g), (4h).} \quad (35a)$$

We utilize the SCA technique as mentioned before to tackle the non-convexity of the numerator in (35a), then transform it through the fractional programming into a parametric subtractive form with an introduced parameter λ , and exploit Dinkelbach's method [43] to obtain a solution of λ and \mathbf{p} . The solving sub-algorithm based on Dinkelbach's method is summarized in Algorithm 2.

For given transmit power vector $\mathbf{p}^{(j)}$ and receive beamforming matrix $\mathbf{W}^{(j)}$, the reflecting coefficient matrix Φ can be optimized by solving the following subproblem

$$(P2.2) : \max_{\Phi} \frac{R(\Phi)}{\sum_{k=1}^K P_k^{c(j)} + \sum_{n \in \mathcal{D}} P_n^{d(j)} + (K+2N+1)P_0 + P_{\text{RIS}}(B)}$$

$$\text{s.t. (4b), (4c), (4j).} \quad (36a)$$

Since the denominator in the objective function is a constant, this subproblem (P2.2) can be solved in the same way as in III-C to obtain a solution to Φ .

For given transmit power vector $\mathbf{p}^{(j)}$ and reflecting coefficient matrix $\Phi^{(j)}$, the receive beamforming matrix \mathbf{W} can be optimized by solving the following subproblem

$$(P2.3) : \max_{\mathbf{W}} \frac{R(\mathbf{W})}{\sum_{k=1}^K P_k^{c(j)} + \sum_{n \in \mathcal{D}} P_n^{d(j)} + (K+2N+1)P_0 + P_{\text{RIS}}(B)}$$

$$\text{s.t. (4c), (4i).} \quad (37a)$$

Since the denominator in the objective function is a constant, this subproblem (P2.3) can be solved in the same way as in III-D.

2) *Overall Algorithm with Convergence and Complexity Analyses:* The overall algorithm for solving (P2) is summarized in Algorithm 2. Specifically, the RCS-based algorithm is exploited to determine the spectrum reuse

Algorithm 2 Proposed algorithm for solving (P2)

Step 1: Initialize $\mathbf{p}^{(0)}$, $\Phi^{(0)}$, $\mathbf{W}^{(0)}$, $\lambda^{(0)} = 0$, permissible error $\delta = 10^{-3}$, a small threshold constant $\epsilon = 10^{-2}$. Let $i = 0$, $j = 0$.

Step 2: Exploit RCS-based pairing scheme to determine the spectrum reuse indicator vector ρ^* .

repeat

Step 3: Solve (P2.1) for given $\Phi^{(j)}$ and $\mathbf{W}^{(j)}$, and obtain the optimal solution as $\mathbf{p}^{(j+1)}$.

repeat

3.1: Solve the following optimization problem to obtain the optimal transmit power $\mathbf{p}^{*(i)}$

$$\max_{\mathbf{p}} f(\lambda^{(i)}) = R^{\text{lb}(i)} - \lambda^{(i)} \left(\sum_{k=1}^K P_k^{c(i)} + \sum_{n \in \mathcal{D}} P_n^{d(i)} + (K+2N+1)P_0 + P_{\text{RIS}}(B) \right)$$

3.2: Update the introduced parameter with $\lambda^{(i)} = \frac{R^{\text{lb}(i)}(\mathbf{p}^{*(i)})}{\sum_{k=1}^K P_k^{c*(i)} + \sum_{n \in \mathcal{D}} P_n^{d*(i)} + (K+2N+1)P_0 + P_{\text{RIS}}(B)}$

3.3: Update iteration index $i = i + 1$.

until $f(\lambda) < \delta$

return $\mathbf{p}^{(j+1)} = \mathbf{p}^{*(i-1)}$.

Step 4: Solve (P2.2) for given $\mathbf{p}^{(j+1)}$ and $\mathbf{W}^{(j)}$, and obtain the optimal solution as $\Phi^{(j+1)}$.

Step 5: Solve (P2.3) for given $\mathbf{p}^{(j+1)}$ and $\Phi^{(j+1)}$, and obtain the optimal solution as $\mathbf{W}^{(j+1)}$.

Step 6: Update iteration index $j = j + 1$.

until The increase of objective value is smaller than ϵ .
Step 7: Return the suboptimal solution ρ^* , $\mathbf{p}^* = \mathbf{p}^{(j-1)}$, $\Phi^* = \Phi^{(j-1)}$ and $\mathbf{W}^* = \mathbf{W}^{(j-1)}$.

indicator ρ , and subproblem (P2.1), (P2.2) and (P2.3) are alternatively solved in each outer-layer iteration.

Theorem 2. *Algorithm 2 is guaranteed to converge.*

Proof: (Sketch) The Dinkelbach's method is used to solve subproblem (P2.1) in Step 3. Since the Dinkelbach's method converges superlinearly for nonlinear fractional programming problems [43], the convergence of Algorithm 2 can be proved by similar steps as in the proof of Theorem 1, and is omitted for brevity. ■

The number of iterations required for Dinkelbach's method's convergence is $\mathcal{O}(\log_2(\frac{1}{\delta}))$, where δ is the permissible error [43]. Each iteration of the proposed Dinkelbach's method solves a convex optimization problem, and the complexity of each iteration is $\mathcal{O}((N+K)^3)$ [40]. (P2.2) and (P2.3) can be transformed as convex QCQPs which can be solved using interior point methods with complexity $\mathcal{O}(M^{3.5})$ and $\mathcal{O}(Q^{3.5})$, respectively. [41]. Hence, the complexity of Algorithm 2 is $\mathcal{O}(I_{\text{ite}} [\log_2(\frac{1}{\delta})(N+K)^3 + M^{3.5} + Q^{3.5}])$, where I_{ite} denotes the number of outer-layer AO iterations. As numerically shown later in Section V, I_{ite} takes the typical

value of 5 in general.

V. NUMERICAL RESULTS

This section provides numerical results for the RIS-empowered D2D underlying a cellular network, which show significant performance enhancement of the proposed design as compared to the conventional underlay D2D network without RIS and other benchmarks.

A. Simulation Setups

Each channel response consists of a large-scale fading component and a small-scale fading component. Without loss of generality, the large-scale fading is distance-dependent and can be modeled as $Cd^{-\alpha}$, where d is the distance between transmitter and receiver with unit of meter (m), $C = 10^{-3}$ is the path loss at the reference distance of 1 m, and α is the path loss exponent of the channel. The path loss exponents from TXs/CUs to RXs/BS are $\alpha = 4$, from IRS to BS is $\alpha = 2$, and for other RIS-related channels we have $\alpha = 2.2$ [14] [27]. Following the literature [24] [27] [36] [44], the small-scale fading components $h_{l,i}$, \mathbf{u}_i , $\tilde{\mathbf{h}}_k$ and $v_{l,k}$ are considered as independently Rayleigh fading distributed⁶, while the small-scale fading components of \mathbf{f}_i , $\tilde{\mathbf{f}}_k$, \mathbf{g}_l and $\tilde{\mathbf{G}}$ follow independent Rician fading distribution, i.e.,

$$\mathbf{f}_i = \sqrt{\frac{K_1}{K_1 + 1}} \mathbf{f}_{L,i} + \sqrt{\frac{1}{K_1 + 1}} \mathbf{f}_{N,i}, \quad (38)$$

where K_1 is the Rician factor of \mathbf{f}_i , $\mathbf{f}_{N,i}$ is the non-LoS (NLoS) component where each element follows CSCG distribution $\mathcal{CN}(0, 1)$, and $\mathbf{f}_{L,i}$ is the line of sight (LoS) component which can be expressed by the steering vector model. $\tilde{\mathbf{f}}_k$, \mathbf{g}_l and $\tilde{\mathbf{G}}$ are generated in the same way as \mathbf{f}_i with Rician factors K_2 , K_3 and K_4 , respectively. Specifically, $\mathbf{f}_{L,i} = \mathbf{a}_M(\theta_1^{\text{AoA}})$, $\tilde{\mathbf{f}}_{L,k} = \mathbf{a}_M(\theta_2^{\text{AoA}})$, $\mathbf{g}_{L,l} = \mathbf{a}_M(\theta_3^{\text{AoD}})$, $\tilde{\mathbf{G}}_L^H = \mathbf{a}_Q(\theta_4^{\text{AoA}}) \mathbf{a}_M^H(\theta_4^{\text{AoD}})$, where $\mathbf{a}_X(\theta) = [1, e^{j\frac{2\pi d}{\lambda_w} \sin \theta}, \dots, e^{j\frac{2\pi d}{\lambda_w} (X-1) \sin \theta}]^T$, $X = \{M, Q\}$, d_a is the antenna spacing, λ_w is the wavelength. θ_1^{AoA} and θ_2^{AoA} are the angle of arrival (AoA) at RIS of (TX i)-to-RIS channel and (CU k)-to-RIS channel; θ_4^{AoA} is the AoA at BS of RIS-to-BS channel; θ_3^{AoD} and θ_4^{AoD} are the angle of departure (AoD) at RIS of RIS-to-(RX 1) channel and RIS-to-BS channel. We generate 1000 channel realizations with independent small-scale fading, and the final results are obtained through averaging the results of these realizations.

We assume that the CUs are uniformly distributed in a circular cell with radius $R = 200$ m. We adopt the clustered distribution model in [14] for D2D users. There are clusters of D2D users randomly distributed in the cell, and each D2D link is uniformly distributed in one cluster with radius $r = 60$ m. We set $K = 6$ and $N = 3$. Since

⁶The channels irrelevant to the RIS can also be assumed to be Rician in general, which do not change the results.

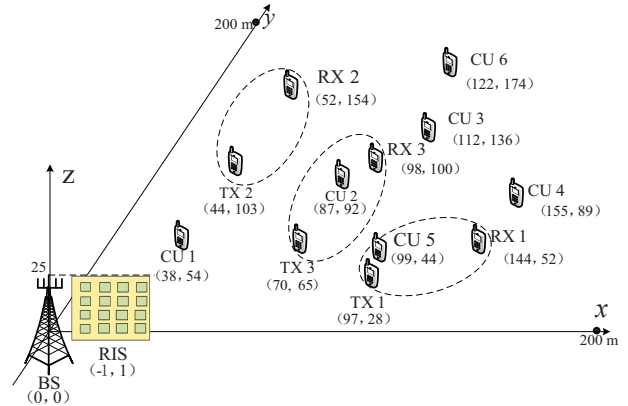


Fig. 2: Topology of RIS-empowered underlay D2D communication network.

the double-fading reflected channel will be better when the RIS is located near the BS or users [12] [24], we deploy the RIS near the BS. The heights of the BS and RIS are 25 m, and the heights of all users are 1.5 m. Using the above method, the locations of CUs and D2D users are generated by one realization, as illustrated in Fig. 2, and then fixed in all the simulations. The simulation results for fixed user locations are given in the following Subsections V-B and V-C, while the system-level simulation results for random user locations are given in Subsection V-D⁷. The power spectral density of noise is -174 dBm/Hz, and the system bandwidth is 1 MHz.

B. SE Simulation Analyses for Fixed User Locations

In this subsection, we evaluate the SE performance. For comparison, we consider the following benchmark schemes.

1) *Underlay D2D Without RIS*: We consider an underlay D2D network without RIS. The SE and EE are maximized by exhaustively searching over A_K^N possible user-pairings and jointly optimizing the transmit power vector \mathbf{p} and the BS's receive beamforming matrix \mathbf{W} under each pairing.

2) *RIS-Empowered D2D With Ideal User Pairing*: We exhaustively search over A_K^N possible user-pairings, and jointly optimize \mathbf{p} together with Φ and \mathbf{W} under each pairing. This benchmark gives achievable upper-bound performance of the RIS-empowered underlay D2D network.

3) *RIS-Empowered D2D With Random Phase Shift*: The user pairing is performed by the proposed RCS-based pairing scheme. We then jointly optimize \mathbf{p} and \mathbf{W} , while Φ is set randomly. This benchmark is utilized to show the benefits of passive beamforming optimization.

⁷For the general case of randomly distributed users in the whole cell, it typically needs to deploy multiple RISs and validate the average performance over multiple drops of user locations. For the considered single-RIS case, the RIS can enhance the communication performance for users in a nearby region, which is set as the right upper quadrant in this paper.

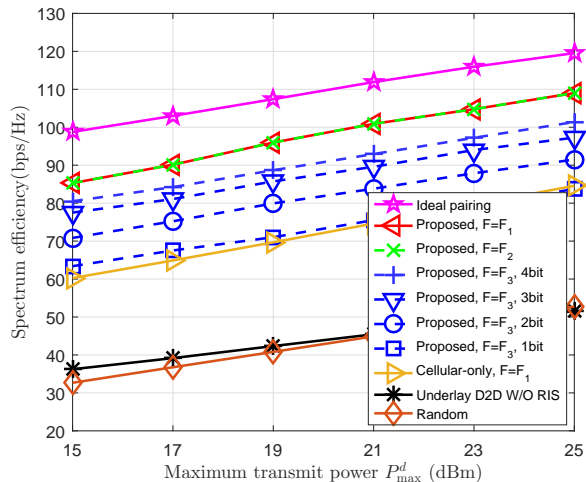


Fig. 3: SE v.s. maximum transmit power P_{\max} .

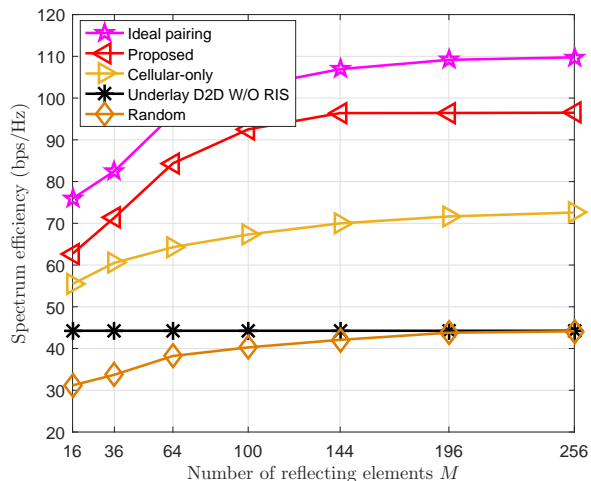


Fig. 4: SE v.s. number of reflecting elements M .

4) *RIS-Empowered cellular-only network*: We consider a pure cellular network without D2D users, where CUs transmit with the maximum power. We jointly optimize Φ and \mathbf{W} to enhance the channel strength between the CUs and the BS. This benchmark can be used to check if the underlay D2D scheme is beneficial for the network's SE and EE.

We set $M = 256$, $P_{\max}^d = P_{\max}^c = 20$ dBm [14], the required rate constraints for D2D users and CUs as $R_{\min}^d = \log_2(1 + \gamma_{\min}^d) = 1$ bps/Hz and $R_{\min}^c = \log_2(1 + \gamma_{\min}^c) = 2$ bps/Hz, respectively, if not specified locally for some figures.

Fig. 3 plots the SE versus the maximum transmit power P_{\max} for the proposed design and different benchmarks. First, the proposed design achieves significant SE enhancement compared to the underlay D2D without RIS.

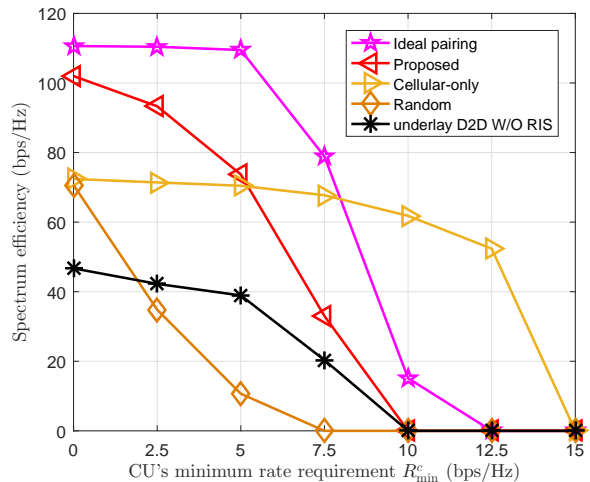
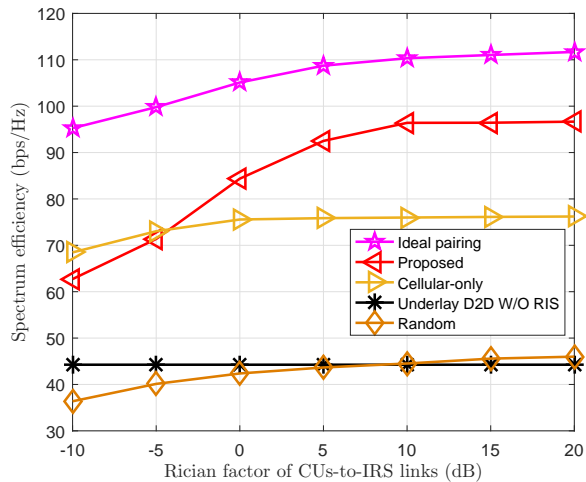


Fig. 5: SE v.s. CU's SINR requirement γ_{\min}^c .

For instance, the SE of the proposed design is 132.43% and 109.62% higher than that of the underlay D2D without RIS, for $P_{\max} = 15, 25$ dBm, respectively. Also, the proposed design outperforms the random phase shift benchmark, which validates the significance of passive beamforming optimization. Then, compared to the ideal pairing benchmark, the proposed design suffers from slight SE performance degradation, but obviously outperforms this benchmark in computational complexity. The proposed design solves the joint resource-allocation optimization problem only once, while this benchmark needs to solve such problem for A_K^N times under all possible pairings, resulting into unaffordable complexity especially for large numbers of D2D or cellular links. Moreover, the network with underlay D2D scheme achieves higher SE than that with cellular-only scheme, which indicates that the superiority of the underlay D2D scheme.

Fig. 3 also shows that the finite-resolution phase shifters of the reflecting elements degrade the SE performance. The SE increases with the phase-shift quantization bits B , since the realized reflecting coefficients approximate their optimal values for larger B . In particular, the 3-bit phase shifters can obtain sufficiently high performance gain with a slight performance degradation compared to the ideal case of continuous phase shifters. Furthermore, the SE of the proposed design with $\mathcal{F} = \mathcal{F}_2$ is almost the same as the proposed design with $\mathcal{F} = \mathcal{F}_1$. Numerical results show that the reflecting amplitudes take the maximal value 1 for $\mathcal{F} = \mathcal{F}_1$, since the channel strength enhancement and inter-link interference suppression can be achieved to the greatest extent by adjusting the reflecting phase shifts.

Fig. 4 plots the SE versus the number of reflecting elements M of the RIS. First, the SE of proposed design increases as M increases, since more reflecting elements can further enhance equivalent channel strength and suppress the inter-link interference; while the SE of the underlay

Fig. 6: SE v.s. Rician factor K_4 .

D2D without RIS almost remains unchanged. Then, we observe that the gap between the proposed design and the ideal pairing benchmark enlarges with the increase of M . The reason is that larger M affects the reflecting channel strength to a greater extent; whereas the RCS-based pairing scheme considers the channel strength of the direct links exclusively, which does not take advantage of the reflecting channel information. Moreover, compared to the ideal pairing benchmark with extremely high complexity, the proposed design achieves 86.59% and 88.18% SE performance of the ideal pairing benchmark (upper bound) when M is 36 and 256, respectively.

Fig. 5 plots the SE versus the CUs' minimum rate requirement R_{\min}^c . The SE decreases as R_{\min}^c increases, which reveals the rate tradeoff between D2D links and cellular links. When R_{\min}^c is relatively small, the proposed design achieves significant SE enhancement by introducing an RIS as compared to the underlay D2D without RIS and the cellular-only benchmark. When R_{\min}^c is relatively large, both the proposed design and the underlay D2D without RIS achieve low SE, while the ideal pairing benchmark and cellular-only benchmark achieve satisfactory SE performance. The reason is that both the pairing scheme and the benefits introduced by the RIS affect the SE performance. When R_{\min}^c is relatively large, the formulated problem is likely to be unsolved under a suboptimal pairing scheme for the proposed design; nevertheless, the ideal pairing scheme can obtain an optimal pairing scheme, and the cellular-only scheme has more relaxed constraints without the minimum rate requirement of the D2D users.

Fig. 6 plots the SE versus the Rician factor K_4 for the BS-to-RIS channel. It is observed that the SE of the proposed design increases as K_4 increases, since larger K_4 indicates stronger LoS path and thus lower probability of deep channel fading. Furthermore, the slope of the curve decreases with K_4 . When K_4 is small (e.g., less than 5

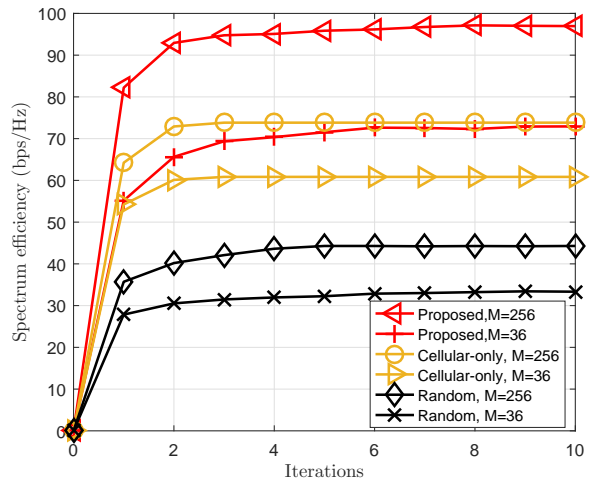
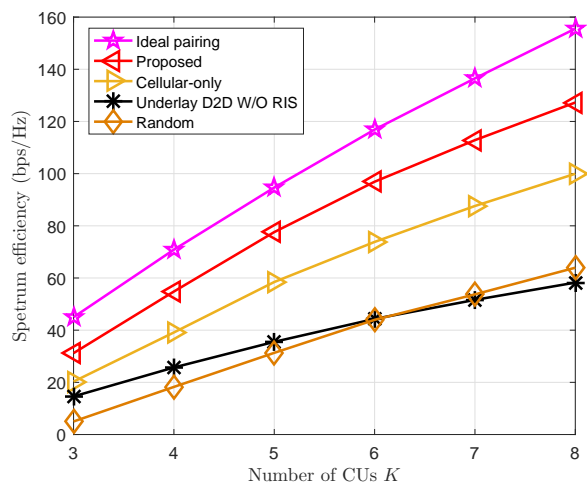


Fig. 7: Convergence of Algorithm 1 for (P1).

Fig. 8: SE v.s. the number of CUs K .

dB), NLoS path is dominant and the effect of enhanced LoS-path strength from increasing K_4 is obvious; when K_4 is relatively large (e.g., 10 dB above), the LoS path is absolutely dominant and K_4 has little effect on the channel. The SE of the underlay D2D without RIS almost remains unchanged.

Fig. 7 plots the average convergence performance of the proposed Algorithm 1. We observe that the proposed scheme takes about five iterations to converge. Each iteration takes about one minute. Thus, the convergence speed of Algorithm 1 is fast. For example, the converged average SE is 98.02 bps/Hz and 72.13 bps/Hz for the proposed design, when M is 256 and 36, respectively.

Fig. 8 plots the SE versus the number of CUs. We set the coordinates of added CUs as (138, 162) and (74, 121) respectively. The proposed design significantly outperforms the underlay D2D without RIS when the number of CUs is relatively large. The reason is explained as follows. With

TABLE I: Power consumption (mW) of each reflecting element.

$M \backslash B$	1	2	3	4	5	6	7	8	9	10
200	5.970	6.000	6.060	6.180	6.420	6.900	7.860	9.780	13.620	21.300
500	2.406	2.436	2.496	2.616	2.856	3.336	4.296	6.216	10.056	17.736
1000	1.218	1.248	1.308	1.428	1.668	2.148	3.108	5.028	8.868	16.548

the number of CUs increases, the SE performance for the underlay D2D without RIS only benefits from the potential better pairing and the rate of added CUs, while the SE performance for the proposed design also benefits from the enhancement of the RIS.

C. EE Simulation Analyses for Fixed User Locations

In this subsection, we evaluate the EE performance. For comparison, we consider the aforementioned three benchmark, and further consider a relay-assisted underlay D2D network, where an amplify-and-forward (AF) relay equipped with M antennas is located at the position of the RIS. The notations remain unchanged. Both the signals from CUs and D2D TXs can be amplified and forwarded through the AF relay. Denote the AF matrix by \mathbf{W}_r . The relay transmit power is

$$P_{AF} = \sum_{n \in \mathcal{D}} P_n^d \|\mathbf{W}_r \mathbf{f}_n\|^2 + \sum_{k=1}^K P_k^c \|\mathbf{W}_r \tilde{\mathbf{f}}_k\|^2 + \sigma^2 \|\mathbf{W}_r\|_F^2. \quad (39)$$

The SINR for RX n decoding s_n from D2D TX n , and for BS decoding x_k from CU k are

$$\hat{\gamma}_n^d = \frac{P_n^d |\mathbf{g}_n^H \mathbf{W}_r \mathbf{f}_n + h_{n,n}|^2}{\sum_{k=1}^K \rho_{k,n} P_k^c |\mathbf{g}_n^H \mathbf{W}_r \tilde{\mathbf{f}}_k + v_{n,k}|^2 + \sigma^2 \|\mathbf{g}_n^H \mathbf{W}_r\|^2 + \sigma^2}, \quad (40a)$$

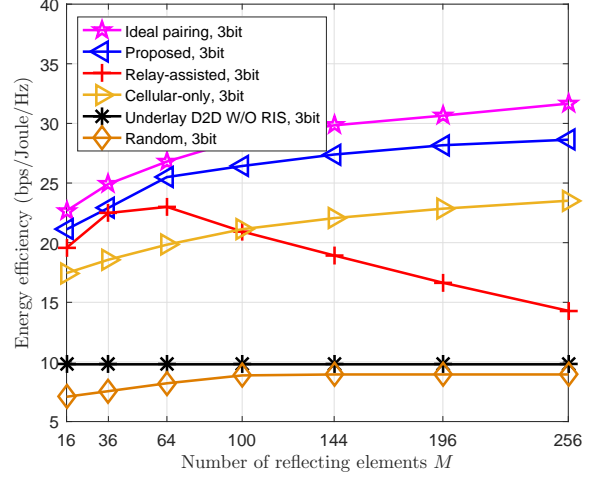
$$\hat{\gamma}_k^c = \frac{P_k^c |\mathbf{w}_k (\tilde{\mathbf{G}}^H \mathbf{W}_r \tilde{\mathbf{f}}_k + \tilde{\mathbf{h}}_k)|^2}{\sum_{i=1}^N \rho_{k,i} P_i^d |\mathbf{w}_k \tilde{\mathbf{G}}^H \mathbf{W}_r \mathbf{f}_i + \mathbf{u}_i|^2 + \sigma^2 (\|\mathbf{w}_k \tilde{\mathbf{G}}^H \mathbf{W}_r\|^2 + \|\mathbf{w}_k\|^2)}. \quad (40b)$$

The EE maximization problem in relay-assisted D2D network is

$$(P3) : \max_{\rho, \mathbf{P}, \mathbf{W}_r, \mathbf{W}} \frac{\sum_{n \in \mathcal{D}} \log_2(1 + \hat{\gamma}_n^d) + \sum_{k=1}^K \log_2(1 + \hat{\gamma}_k^c)}{\sum_{k=1}^K P_k^c + \sum_{n \in \mathcal{D}} P_n^d + (K + 2N + 1)P_0 + P_{AF}} \quad (41a)$$

$$\text{s.t. (4b), (4c), (4d), (4e), (4f), (4g), (4h), (4i).} \quad (41b)$$

$$\sum_{n \in \mathcal{D}} P_n^d \|\mathbf{W}_r \mathbf{f}_n\|^2 + \sum_{k=1}^K P_k^c \|\mathbf{W}_r \tilde{\mathbf{f}}_k\|^2 + \sigma^2 \|\mathbf{W}_r\|_F^2 \leq P_{r,\max}, \quad (41c)$$

Fig. 9: EE v.s. number of reflecting elements M .

where $P_{r,\max}$ is the maximum transmit power of the AF relay. The structures of $\hat{\gamma}_n^d$ and $\hat{\gamma}_k^c$ are the same as (1) and (2), respectively, an algorithm analogous to Algorithm 2 is utilized to solve (P3).

As in [36], we take the diode SMV1231-079 with inverse current less than 20 nA, and estimate the power $P_v(B)$ for different B 's. We take the typical Xilinx Spartan-7 FPGA for consideration, and use its typical power $P_{FPGA} = 1.188$ W. The average power consumption of each reflecting element for different quantization bit B with reflecting-element number M is given in Table I. In the simulations, we set $M = 256$, $R_{\min}^d = 1$ bps/Hz and $R_{\min}^c = 2$ bps/Hz, $P_r = 20$ dBm, $P_{r,\max} = 6$ W, $f_s = 10$ KHz, and the dissipated power at each AF relay transmit-receive antenna is 10 dBm. The bias voltages of varactor diode are chosen in the range of [0.12, 8.83]. Other settings remain unchanged as in subsection VI-C.

Fig. 9 plots the EE versus the number of reflecting elements M . For the proposed design, EE increases as P_{\max} increases first, then almost remains unchanged for large M , since the increment of SE is not as fast as the increment of power consumption. The proposed design significantly outperforms the underlay D2D without RIS. The proposed design also achieves far better EE performance than the random phase shift benchmark, which shows the great significance of passive beamforming optimization. Moreover,

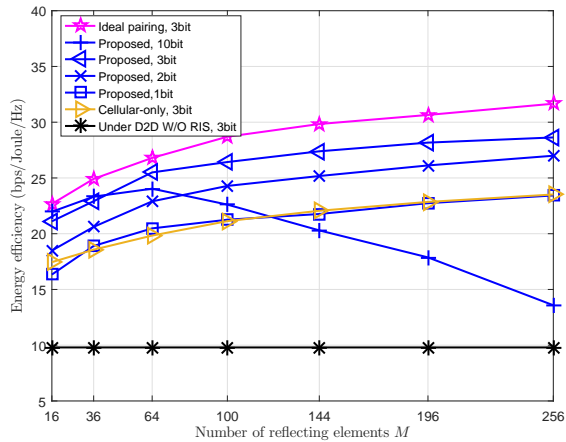


Fig. 10: EE v.s. M for different B .

the proposed design suffers from slight EE performance degradation, but outperforms the ideal pairing benchmark in terms of computational complexity. For relay-assisted underlay D2D, EE increases first and then decreases. The reason is as follows. The increment of M makes the AF beamforming more accurate. When M is small, the introduced larger noise power and higher AF relay energy consumption due to increasing M is negligible, thus the benefit from accurate AF beamforming is obvious; when M is relatively large, the introduced noise power and AF relay energy consumption are large enough, which cause the decrement of the EE performance. Moreover, the network with underlay D2D scheme achieves higher EE than that with cellular-only scheme, which indicates that the superiority of the underlay D2D scheme.

Fig. 10 plots the EE versus the number of reflecting elements M for different phase-shift quantization bits B . With fixed $M = 100$, it is observed that as the number of phase-shift quantization bits B increases, the EE increases first and then decreases. The reason is that despite the increment of B makes the setting of reflecting coefficients more accurate, it results into higher power consumption simultaneously. When B is large enough, the SE improvement from RIS is not enough to compensate for the incremental power consumption as B increases. Moreover, for the proposed design with 10-bits quantization, the EE increases first and then decreases as M increases, which reveals the trade-off between the EE and number of reflecting elements.

Fig. 11 plots the average convergence performance of Dinkelbach-based Algorithm 2 for solving EE-maximization problem (P2). We observe that the proposed design takes about five iterations to converge. Each iteration takes about two minutes. Thus, the convergence of Algorithm 2 is fast. The converged average EE is 27.42 bps/Joule/Hz for the proposed design.

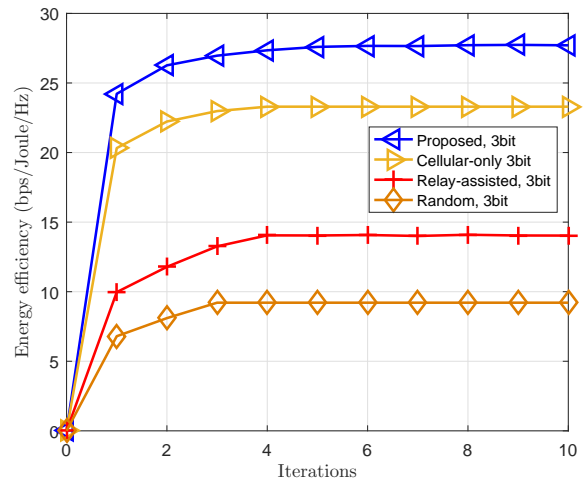


Fig. 11: Convergence of Dinkelbach-based Algorithm 2 for (P2).

D. System-level Simulation Analyses for Random User Locations

We consider system-level simulation in terms of the average performance under random locations of D2D users and CUs. Specifically, we assume the horizontal coordinate and longitudinal coordinate for each user follows independent uniform distribution $U[0, 200]$ m. Fig. 12 plots the average SE versus the maximum transmit power P_{\max} from system level, and Fig. 13 plots the average EE versus the number of reflecting elements M from system level. By comparing Fig. 12 and Fig. 13 with Fig. 3 and Fig. 9 for fixed user locations, respectively, we observe that both SE and EE decrease slightly for each scheme. The reason is that the relative positions of D2D pairs and CUs definitely affect the system performance. However, both the curve trends and the related conclusions still hold.

VI. CONCLUSION

This paper has studied an RIS-empowered underlay D2D communication network. The overall network's spectrum efficiency (SE) and energy efficiency (EE) are maximized, respectively, by jointly optimizing the spectrum reuse indicators, the transmit power, the RIS's passive beamforming and the BS's receive beamforming. An efficient relative-channel-strength based user-pairing scheme with low complexity is first proposed to determine the spectrum reuse indicators. Other variables are then optimized by utilizing the proposed alternating-optimization based iterative algorithms. Numerical results show that the proposed design achieves significant performance enhancement compared to traditional underlay D2D network without RIS, and suffers from slight performance degradation compared to RIS-empowered underly D2D with ideal user-pairing. This work can be extended to practical and complex scenarios

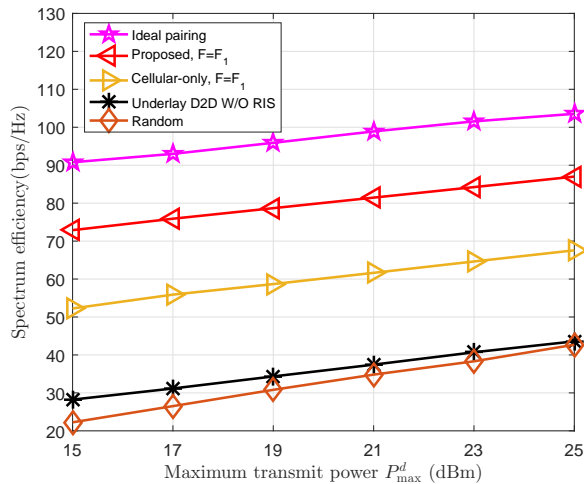


Fig. 12: System-level SE v.s. maximum transmit power P_{\max}^d .

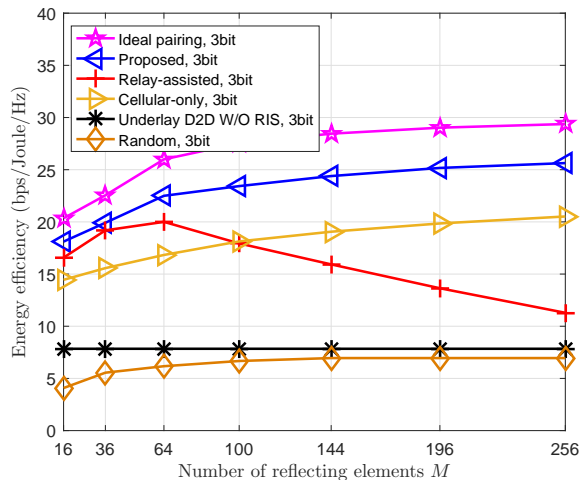


Fig. 13: System-level EE v.s. number of reflecting elements M .

such as multiple RISs and imperfect channel state information.

REFERENCES

- [1] F. Jameel, Z. Hamid, F. Jabeen, S. Zeadally, and M. A. Javed, "A survey of device-to-device communications: Research issues and challenges," *IEEE Commun. Sur. & Tut.*, vol. 20, no. 3, pp. 2133–2168, 2018.
- [2] H. Guo, J. Liu, J. Ren, and Y. Zhang, "Intelligent task offloading in vehicular edge computing networks," *IEEE Wireless Commun.*, vol. 27, no. 4, pp. 126–132, 2020.
- [3] H. Guo, J. Liu, and J. Lv, "Toward intelligent task offloading at the edge," *IEEE Network*, vol. 34, no. 2, pp. 128–134, 2020.
- [4] A. Ghosh, A. Maeder, M. Baker, and D. Chandramouli, "5G evolution: A view on 5G cellular technology beyond 3GPP release 15," *IEEE Access*, vol. 7, pp. 127 639–127 651, 2019.

- [5] Y.-C. Liang, *Dynamic Spectrum Management: From Cognitive Radio to Blockchain and Artificial Intelligence*, ser. Signals and Communication Technology. Singapore: Springer, 2020.
- [6] J. Wang, Y. Huang, S. Jin, R. Schober, X. You, and C. Zhao, "Resource management for device-to-device communication: A physical layer security perspective," *IEEE J. Sel. Areas Commun.*, vol. 36, no. 4, pp. 946–960, 2018.
- [7] K. Yang, S. Martin, C. Xing, J. Wu, and R. Fan, "Energy-efficient power control for device-to-device communications," *IEEE J. Sel. Areas Commun.*, vol. 34, no. 12, pp. 3208–3220, 2016.
- [8] C. Liaskos, S. Nie, A. Tsioliaridou, A. Pitsillides, S. Ioannidis, and I. Akyildiz, "A new wireless communication paradigm through software-controlled metasurfaces," *IEEE Commun. Mag.*, vol. 56, no. 9, pp. 162–169, 2018.
- [9] M. Di Renzo, M. Debbah, and et. al., "Smart radio environments empowered by reconfigurable AI meta-surfaces: an idea whose time has come," *EURASIP J. Wireless Commun. Netw.*, vol. 2019, no. 1, pp. 1–20, 2019.
- [10] Y.-C. Liang, R. Long, Q. Zhang, J. Chen, H. V. Cheng, and H. Guo, "Large intelligent surface/antennas (LISA): Making reflective radios smart," *J. Commun. Inf. Netw.*, vol. 4, no. 2, pp. 40–50, 2019.
- [11] C. Huang, S. Hu, G. C. Alexandropoulos, A. Zappone, C. Yuen, R. Zhang, M. Di Renzo, and M. Debbah, "Holographic MIMO surfaces for 6G wireless networks: Opportunities, challenges, and trends," *IEEE Wireless Commun.*, vol. 27, no. 5, pp. 118–125, 2020.
- [12] E. Björnson, O. Özdogan, and E. G. Larsson, "Intelligent reflecting surface versus decode-and-forward: How large surfaces are needed to beat relaying?" *IEEE Wireless Commun. Lett.*, vol. 9, no. 2, pp. 244–248, 2020.
- [13] S. Jia, X. Yuan, and Y.-C. Liang, "Reconfigurable intelligent surfaces for energy efficiency in D2D communication network," *IEEE Wireless Commun. Lett.*, vol. 10, no. 3, pp. 683–687, 2021.
- [14] D. Feng, L. Lu, Y. Yuan-Wu, G. Y. Li, G. Feng, and S. Li, "Device-to-device communications underlaying cellular networks," *IEEE Trans. Commun.*, vol. 61, no. 8, pp. 3541–3551, 2013.
- [15] Y. Kai, J. Wang, H. Zhu, and J. Wang, "Resource allocation and performance analysis of cellular-assisted OFDMA device-to-device communications," *IEEE Trans. Wireless Commun.*, vol. 18, no. 1, pp. 416–431, 2019.
- [16] W. Cui, K. Shen, and W. Yu, "Spatial deep learning for wireless scheduling," *IEEE J. Sel. Areas Commun.*, vol. 37, no. 6, pp. 1248–1261, 2019.
- [17] J. Mirza, G. Zheng, K. Wong, and S. Saleem, "Joint beamforming and power optimization for D2D underlaying cellular networks," *IEEE Trans. Veh. Technol.*, vol. 67, no. 9, pp. 8324–8335, 2018.
- [18] F. Wang, C. Xu, L. Song, and Z. Han, "Energy-efficient resource allocation for device-to-device underlay communication," *IEEE Trans. Wireless Commun.*, vol. 14, no. 4, pp. 2082–2092, 2015.
- [19] D. Feng, G. Yu, C. Xiong, Y. Yuan-Wu, G. Y. Li, G. Feng, and S. Li, "Mode switching for energy-efficient device-to-device communications in cellular networks," *IEEE Tran. Wireless Commun.*, vol. 14, no. 12, pp. 6993–7003, 2015.
- [20] Y. J. Chun, S. L. Cotton, H. S. Dhillon, A. Ghayeb, and M. O. Hasna, "A stochastic geometric analysis of device-to-device communications operating over generalized fading channels," *IEEE Trans. Wireless Commun.*, vol. 16, no. 7, pp. 4151–4165, 2017.
- [21] M. Di Renzo, A. Zappone, M. Debbah, M. S. Alouini, C. Yuen, J. de Rosny, and S. Tretyakov, "Smart radio environments empowered by reconfigurable intelligent surfaces: How it works, state of research, and the road ahead," *IEEE J. Sel. Areas Commun.*, vol. 38, no. 11, pp. 2450–2525, 2020.
- [22] G. Yang, Y.-C. Liang, R. Zhang, and Y. Pei, "Modulation in the air: Backscatter communication over ambient OFDM carrier," *IEEE Trans. Commun.*, vol. 66, no. 3, pp. 1219–1233, Mar. 2018.
- [23] G. Yang, Q. Zhang, and Y.-C. Liang, "Cooperative ambient backscatter communications for green Internet-of-Things," *IEEE Internet of Things J.*, vol. 5, no. 2, pp. 1116–1130, Apr. 2018.
- [24] H. Guo, Y.-C. Liang, J. Chen, and E. G. Larsson, "Weighted sum-rate maximization for reconfigurable intelligent surface aided wireless networks," *IEEE Tran. Wireless Commun.*, vol. 19, no. 5, pp. 3064–3076, 2020.

- [25] C. Huang, R. Mo, and C. Yuen, "Reconfigurable intelligent surface assisted multiuser MISO systems exploiting deep reinforcement learning," *IEEE J. Sel. Areas Commun.*, vol. 38, no. 8, pp. 1839–1850, 2020.
- [26] G. Yang, X. Xu, Y. C. Liang, and M. Di Renzo, "Reconfigurable intelligent surface assisted non-orthogonal multiple access," *IEEE Trans. on Wireless Commun.*, vol. 20, no. 5, pp. 3137–3151, 2021.
- [27] C. Huang, A. Zappone, G. C. Alexandropoulos, M. Debbah, and C. Yuen, "Reconfigurable intelligent surfaces for energy efficiency in wireless communication," *IEEE Trans. Wireless Commun.*, vol. 18, no. 8, pp. 4157–4170, 2019.
- [28] G. Yang, Y. Liao, Y.-C. Liang, and O. Tirkkonen, "Reconfigurable intelligent surface empowered underlaying device-to-device communication," in *IEEE Wireless Commun. Netw. Conf. (WCNC), Nanjing, China*, 2021.
- [29] M. Alnakhli, S. Anand, and R. Chandramouli, "Joint spectrum and energy efficiency in device to device communication enabled wireless networks," *IEEE Trans. Cognitive Commun. Netw.*, vol. 3, no. 2, pp. 217–225, 2017.
- [30] J. Zhao, "Optimizations with intelligent reflecting surfaces (IRSs) in 6G wireless networks: Power control, quality of service, max-min fair beamforming for unicast, broadcast, and multicast with multi-antenna mobile users and multiple IRSs," online available in Arxiv: arXiv:1908.03965.
- [31] A. Ramezani-Kebrya, M. Dong, B. Liang, G. Boudreau, and S. H. Seyedmehdi, "Joint power optimization for device-to-device communication in cellular networks with interference control," *IEEE Trans. Wireless Commun.*, vol. 16, no. 8, pp. 5131–5146, 2017.
- [32] Z. Wang, L. Liu, and S. Cui, "Channel estimation for intelligent reflecting surface assisted multiuser communications: Framework, algorithms, and analysis," *IEEE Trans. Wireless Commun.*, vol. 19, no. 10, pp. 6607–6620, 2020.
- [33] A. Taha, M. Alrabeiah, and A. Alkhateeb, "Enabling large intelligent surfaces with compressive sensing and deep learning," *IEEE Access, Early Access*, 2021.
- [34] G. Zhou, C. Pan, H. Ren, K. Wang, and A. Nallanathan, "A framework of robust transmission design for IRS-aided MISO communications with imperfect cascaded channels," *IEEE Trans. on Signal Processing*, vol. 68, pp. 5092–5106, 2020.
- [35] Y. Liu, J. Zhao, M. Li, and Q. Wu, "Intelligent reflecting surface aided MISO uplink communication network: Feasibility and power minimization for perfect and imperfect CSI," *IEEE Trans. on Commun.*, vol. 69, no. 3, pp. 1975–1989, 2021.
- [36] S. Abeywickrama, R. Zhang, Q. Wu, and C. Yuen, "Intelligent reflecting surface: Practical phase shift model and beamforming optimization," *IEEE Trans. Commun.*, vol. 68, no. 9, pp. 5849–5863, 2020.
- [37] A. Beck, A. Ben-Tal, and L. Tretuashvili, "A sequential parametric convex approximation method with applications to nonconvex truss topology design problems," *J. Global Opt.*, vol. 47, no. 1, pp. 29–51, 2010.
- [38] M. Grant, S. Boyd, and Y. Ye, "CVX: Matlab software for disciplined convex programming," 2008.
- [39] K. Shen and W. Yu, "Fractional programming for communication systems part I: power control and beamforming," *IEEE Trans. Signal Processing*, vol. 66, no. 10, pp. 2616–2630, 2018.
- [40] D. Bharadia, G. Bansal, P. Kaligineedi, and V. K. Bhargava, "Relay and power allocation schemes for OFDM-based cognitive radio systems," *IEEE Trans. Wireless Commun.*, vol. 10, no. 9, pp. 2812–2817, 2011.
- [41] A. Hassaniien, S. A. Vorobyov, and K. M. Wong, "Robust adaptive beamforming using sequential quadratic programming: An iterative solution to the mismatch problem," *IEEE Signal Processing Lett.*, vol. 15, pp. 733–736, 2008.
- [42] L. N. Ribeiro, S. Schwarz, M. Rupp, and A. L. F. de Almeida, "Energy efficiency of mmwave massive MIMO precoding with low-resolution DACs," *IEEE J. Sel. Topics in Sig. Proc.*, vol. 12, no. 2, pp. 298–312, 2018.
- [43] J.-P. Crouzeix and J. A. Ferland, "Algorithms for generalized fractional programming," *Math. Programm.*, vol. 52, no. 1-3, pp. 191–207, 1991.
- [44] J. Chen, Y.-C. Liang, Y. Pei, and H. Guo, "Intelligent reflecting surface: A programmable wireless environment for physical layer security," *IEEE Access*, vol. 7, pp. 82599–82612, 2019.